Theses and Dissertations

1-1-2013

Depairing Current Density In Cuprate Superconductors

Manlai Liang
University of South Carolina - Columbia

Follow this and additional works at: http://scholarcommons.sc.edu/etd

Depairing Current Density in Cuprate Superconductors

by

Manlai Liang

Bachelor of Science
University of Science and Technology of China, 2008

Submitted in Partial Fulfillment of the Requirements

for the Degree of Doctor of Philosphy in

Physics

College of Arts and Sciences

University of South Carolina

2013

Accepted by:

Milind N. Kunchur, Major Professor

James M. Knight, Committee Member

Scott R. Crittenden, Committee Member

Grigory Simin, Committee Member and External Examiner

Lacy Ford, Vice Provost and Dean of Graduate Studies

ACKNOWLEDGMENTS

Abstract

We report a study of the depairing critical current density in the electron-doped infinite-layer $Sr_{1-x}La_xCuO_2$ and $Nd_{2-x}Ce_xCuO_{4-\delta}$ system. In this work, many new apparatuses were set up to measure the samples. Resistance-versus-temperature transition curves measured at high pulsed current densities show the classic proportionality between the transition-temperature shift and the two-thirds power of the applied current. The measurement provides an assessment of the superfluid density in the system, and a secondary route for obtaining the penetration depth purely through a transport measurements.

Table of Contents

List of Tables

LIST OF FIGURES

INTRODUCTION

A superconductor is a material in which charge carriers condense into a macroscopic quantum state and is characterized by two intrinsic properties: zero resistance and perfect diamagnetism, when its temperature is below a characteristic transition temperature T_c. The phenomenon of zero electric resistance was discovered in 1911 by H. K. Onnes [46] when he cooled the element mercury to below 4.15 K. He also found that a sufficiently strong magnetic field applied on a superconductor can destroy the resistanceless state. However, the perfect diamagnetism was not found until 25 years later when Meissner and Ochsenfeld put a superconducting sphere into a magnetic field and found that it repelled all the magnetic flux [44], namely the Meissner effect.

The progress of searching for higher T_c superconductors used to be very slow. In the 70 years after the discovery of superconductivity, the highest known T_c was only 23K for Nb_3Ge, found by Gavaler [16]. This situation was finally changed when the cuprate superconductor was discovered by Bednorz and Müller [5] in 1986. The transition temperature they found for the compound of lanthanum, barium, and copper reached ~ 35K. The very next year, the record of T_c was quickly boosted up to ~ 90K with the discovery of $YBa_2Cu_3O_{7-x}$ (YBCO) [65, 26, 66]. Since then, more cuprate superconductors have been created by scientists [23]. It's also very interesting to see that superconductivity was found in the iron-based compound by Kamihara et al. [28] in 2006, since iron has a strong local magnetic moment which was thought to be destructive to superconductivity [55, 21].

In contrast to the hole-doped cuprate superconductors such as YBCO, the n-type superconductor that was found in 1989 [56, 58] is electron-doped. For example, in the

mostly studied $Nd_{2-x}Ce_xCuO_4$, Ce^{4+} takes the place of Nd^{3+}, that contributes one extra electron to the copper-oxygen plane. These kinds of cuprate superconductors are currently few in number, but they are important for understanding the whole family of cuprate compounds. However, the electron-doped materials have much fewer measurements than the p-type ones [1].

The current theoretical interpretation of superconductivity is based on a microscopic theory which was presented by Bardeen, Cooper, and Schrieffer(BCS) in 1957 [4]. In this framework, the authors assume the electrons condense into pairs as the current carriers. The binding of these pairs originates from the electron-phonon mechanism inside a superconductor which was first understood by the isotope effect [14]. Additionally, the phenomenological Ginzburg-Landau theory [18](1950), which was frequently used near T_c because it's more easily handled, can be derived from the BCS formalism [19]. However, it remains controversial whether the BCS theory can work well in the high temperature superconductors, such as cuprate superconductors. Researchers are also interested in seeing if the recently-found iron-based superconductors may help in the development of a new non-BCS theory.

The superconducting state will collapse immediately if any one of three prime parameters reaches its critical value: temperature T, applied magnetic field B and current density j. The phase diagrams of $B - T$, $T - j$ and $B - j$ will determine the phase transitions of the superconductors. These three parameters represent three different energies: T for thermal energy, B for magnetic-field expulsion and j for kinetic energy. The phase transition will occur when the superconducting energy gap or the binding energy of electron pairs is overcome by one or more of the three energies. Therefore, it's essential to study the transition curve in variation with T, B and j to understand the primary properties of the superconductors.

Superconductors can be classified into two different types based on their performance under a magnetic field. Those superconductors that can keep the resistance-

less state and exclude all the magnetic flux until the magnetic field goes beyond the specific value, critical field B_c, are known as Type I superconductors. The other superconductors, Type II superconductors, will exhibit more complicated magnetic properties under the field. They show a perfect Meissner effect when the field is low. But the flux can partially penetrate into the superconductor body in the form of vortex, when the strength of magnetic field increases over the first critical field B_{c1}. This mixed state holds until the field exceeds the value of the second critical field B_{c2}. After that, the superconductor will return to the normal state.

Besides the magnetic field, the current can also alter the state of a superconductor due to it suppressing the superconducting energy gap. When the current density is low, type I superconductors remain in perfect conduction. For type II superconductors in a mixed state, the vortex feels a Lorentz force that is perpendicular to the direction and proportional to the magnitude of current. However, if the current is low enough, the dissipation from the motion of vortex is little since most of the vortices are pinned in the defects of the lattice, namely pinning centers. If the current is increased up to a critical value, the Lorentz force overcomes the pinning force and then the pinned vortices will be released and moving. A significant resistance can be observed. That critical value is called the critical current density j_c for type II superconductors. j_c also means the critical current which destroys the superconductivity in type I superconductors since the resistivity rises rapidly when the current goes beyond it. Further increase of the current brings the kinetic energy of the electrons up to the condensation energy. This depairing or pair-breaking current density j_d turns the system into normal state.

In this work, high current density pulses were applied to two n-type cuprate films, $Sr_{1-x}La_xCuO_2$ (SLCO) and $Nd_{2-x}Ce_xCuO_{4-\delta}$ (NCCO). In this regime, the superconducting energy gap will be strongly suppressed and j_d could be found. The upper critical fields were also measured. The principal physical quantity that we

measured is the transition temperature, in variation with current and magnetic field, and yields the necessary information about the nature of the superconductivity. To achieve our goals, several devices were built and some new equipment was set up as discussed in Chapter 4. Additionally, a new cryostat was prepared for future anisotropy measurements.

CHAPTER 1

THEORIES OF SUPERCONDUCTIVITY

In this chapter, we review some basic theories of superconductivity, including both macroscopic and microscopic regimes.

1.1 LONDON EQUATIONS

The Meissner effect was first explained by the theory of the brothers F. and L. London [40]. Their equations first built up a relation between the electric field $\mathbf{E}$, magnetic filed $\mathbf{B}$ and current density $\mathbf{j}$ in the superconductor. The first equation they proposed is

$$\mathbf{E} = \mu_0 \lambda_L^2 \frac{d}{dt}\mathbf{j} \tag{1.1}$$

and second one is

$$\mathbf{B} = -\mu_0 \lambda_L^2 \nabla \times \mathbf{j} \tag{1.2}$$

where λ_L is the London penetration depth. These equations can be obtained from the definition of the quantum mechanical electric current as discussed in the section of Ginzburg-Landau theory. The first equation simply means the electric field will always accelerate the carriers inside the superconductor and therefore change the current. If the second equation is substituted into the Maxwell's equation $\mathbf{j} = \frac{1}{\mu_0}\nabla \times \mathbf{B}$, we have

$$\nabla^2 \mathbf{B} = \frac{\mathbf{B}}{\lambda_L^2} \tag{1.3}$$

In case where $\mathbf{B}$ only varies in the z direction, the above equation has the solution $B = B_0 e^{-z/\lambda_L}$. This shows the magnetic field will penetrate into the superconductor

5

only a few λ_L, which is exactly what the Meissner effect describes. λ_L is of order $10^{-6}m$ and has empirical temperature dependence

$$\lambda_L(T)^{-1} \approx \lambda_L(0)^{-1}\sqrt{1 - t^4}. \tag{1.4}$$

It holds when T is close to T_c. Here t is the deduced temperature T/T_c.

1.2 GINZBURG-LANDAU THEORY

A very useful phenomenological theory was proposed by Ginzburg and Landau (GL) [18] in 1950. It starts from defining a complex order parameter ψ, with $|\psi|^2$ being proportional to the number density of superconducting carriers. The theory is based on the free energy of superconductors in terms of $|\psi|^2$ and its gradient $|\nabla\psi|^2$. As a result, this language provides a good tool to understand many complicated situations in superconductors such as magnetic fields, currents and spatial inhomogeneity.

When the temperature is close to T_c, GL assumed ψ and its gradient are small, and the Gibbs free energy density can be defined as

$$g = g_n + a|\psi|^2 + \frac{b}{2}|\psi|^4 + \frac{1}{2m^*}|(-i\hbar\nabla - 2e\mathbf{A})\psi|^2 + \frac{|\mathbf{B}|^2}{2\mu_0} \tag{1.5}$$

where g_n is the free energy density of normal state, m^* is the effective mass of the quasiparticle, a and b are parameters that only depend on temperature, $\mathbf{A}$ is the magnetic vector potential, and $\mathbf{B}$ is the magnetic field.

In the case of no gradient or field,

$$g = g_n + a|\psi|^2 + \frac{b}{2}|\psi|^4 \tag{1.6}$$

When the derivative of g equals zero,

$$a\psi + b\psi|\psi|^2 = 0 \tag{1.7}$$

which gives

$$|\psi_m|^2 = -\frac{a}{b} \tag{1.8}$$

The minimum free energy occurs at $|\psi_m|^2 = -a/b$ only if $a < 0$ and $b > 0$. With this value of ψ, Eq. 1.6 turns out to be

$$g - g_n = -\frac{a^2}{2b} = -\frac{|\mathbf{B_c}|^2}{2\mu_0},\tag{1.9}$$

where we define the maximum value of B, namely thermodynamic critical field $B_c = \mu_0 a^2/b$, where beyond that the superconducting state is destroyed.

Coherence length and penetration depth

To consider the gradient term in the free energy, we first stay in the regime where the order parameter has a constant amplitude ψ_0 everywhere and depends on location only through its phase $\varphi(\mathbf{r})$. In this case, ψ can written in the form

$$\psi(\mathbf{r}) = \psi_0 e^{i\varphi(\mathbf{r})}\tag{1.10}$$

Substitute this into the Eq. 1.5 and take a derivative with respect to ψ,

$$a\psi_0 + b\psi_0^3 + \frac{\hbar^2}{2m^*}\psi_0 e^{-i\varphi}(i\nabla + \frac{2\pi}{\Phi_0}\mathbf{A})^2 e^{i\varphi} = 0,\tag{1.11}$$

where $\Phi_0 = \frac{h}{2e}$ is the fluxoid quantum. If the gradient of the phase is small, the second order term $\nabla^2\varphi$ is negligible. Then it turns out to be

$$a + b\psi_0^2 + \frac{\hbar^2}{2m^*}(\nabla\varphi - \frac{2\pi}{\Phi_0}\mathbf{A})^2 = 0.\tag{1.12}$$

This equation could be used to determine the value of ψ_0. Now let's define the coherence length ξ from the most simple case $\mathbf{A} = 0$ of above equation. Since $a < 0$, we have

$$\frac{\hbar^2}{2m^*|a|}(\nabla\varphi)^2 = 1 - \frac{b}{|a|}\psi_0^2.\tag{1.13}$$

The right hand side (R.H.S.) equals 0 when $\psi_0 = |\psi_m|$. Apparently, the characteristic length of the variance in the phase φ is

$$\xi^2(T) = \frac{\hbar^2}{2m^*|a(T)|} \propto \frac{1}{1-t},\tag{1.14}$$

where the temperature dependence is phenomenological. Another characteristic meaning of the coherence length will be discussed in the following subsection.

In GL theory, the current density is given by [7]

$$\mathbf{j} = -\frac{i\hbar e}{m^*}(\psi^*\nabla\psi - \psi\nabla\psi^*) - \frac{4e^2}{m^*}\mathbf{A}|\psi|^2 \tag{1.15}$$

Then the current density with the assumption Eq. 1.10 will be

$$\mathbf{j} = \frac{2\hbar e}{m^*}\psi_0^2(\nabla\varphi - \frac{2\pi}{\Phi_0}\mathbf{A}) \tag{1.16}$$

From this we have

$$\nabla \times \mathbf{j} = -\frac{4\pi\hbar e\psi_0^2}{m\Phi_0}\nabla \times \mathbf{A} = -\frac{4e^2\psi_0^2}{m^*}\mathbf{B}. \tag{1.17}$$

Comparing this with the second London equation Eq. 1.2, we get the definition of λ_{eff},

$$\lambda_{eff}^2 = \frac{m^*}{4\mu_0 e^2\psi_0^2}. \tag{1.18}$$

In the London framework, $\nabla\varphi = 0$ and $\psi_0 = |\psi_m|$. Therefore

$$\lambda_L^2 = \frac{m^*}{4\mu_0 e^2|\psi_m|^2}. \tag{1.19}$$

$|\psi|^2$ could be defined as the density of superconducting quasiparticles n_s and expressed in λ_{eff}

$$n_s = \frac{m^*}{4\mu_0 e^2\lambda_{eff}^2}. \tag{1.20}$$

Since the penetration depth is much more easily measured and n_s is directly related to the superconducting energy gap, this simple equation provides a useful tool to probe the gap information.

Upper critical field

We already discussed the case of ψ with a constant amplitude ψ_0 under a field. That is valid only in a thin film or wire. Here, we consider another extreme limit: the

magnetic field is large enough so that $|\psi|^2 \ll |\psi_m|^2 = -a/b$. Under this assumption, it's safe to only keep the terms with the lowest order of ψ in the GL free energy Eq. 1.5 and its differential. Taking a derivative of Eq. 1.5 to ψ, one finds [57]

$$(\frac{\nabla}{i} - \frac{2\pi}{\Phi_0}\mathbf{A})^2\psi = -\frac{2m^*a}{\hbar^2}\psi = \frac{\psi}{\xi^2}. \tag{1.21}$$

Setting the field along the z axis with $(A_x, A_y) = (0, Bx)$, we have

$$[-\nabla^2 + i2\frac{2\pi B}{\Phi_0}x\frac{\partial}{\partial y} + (\frac{2\pi B}{\Phi_0})^2x^2]\psi = \frac{\psi}{\xi^2}. \tag{1.22}$$

Since the vector potential depends only on x, the possible form of the solution is

$$\psi = f(x)e^{ik_y y}e^{ik_z z} \tag{1.23}$$

Substitute this into Eq. 1.22,

$$-f'' + (\frac{2\pi B}{\Phi_0})^2(x - x_0)^2f = (\frac{1}{\xi^2} - k_z^2)f \tag{1.24}$$

with $x_0 = k_y\Phi_0/2\pi B$. Using similar techniques in solving the Schrödinger equation for a particle in a harmonic oscillator potential, we get the eigenfunctions

$$f(x) = exp[-\frac{(x - x_0)^2}{2\xi^2}] \tag{1.25}$$

with the eigenvalues

$$B = \frac{\Phi_0}{2\pi(2n + 1)}(\frac{1}{\xi^2} - k_z^2). \tag{1.26}$$

The solution of $f(x)$ shows the amplitude of ψ also varies in a characteristic length of order ξ. The expression of B gives the highest value when $n = 0$ and $k_z = 0$. The maximum value, namely upper critical field, is

$$B_{c2} = \frac{\Phi_0}{2\pi\xi^2}. \tag{1.27}$$

By defining a dimensionless quantity

$$\kappa = \frac{\lambda}{\xi} \tag{1.28}$$
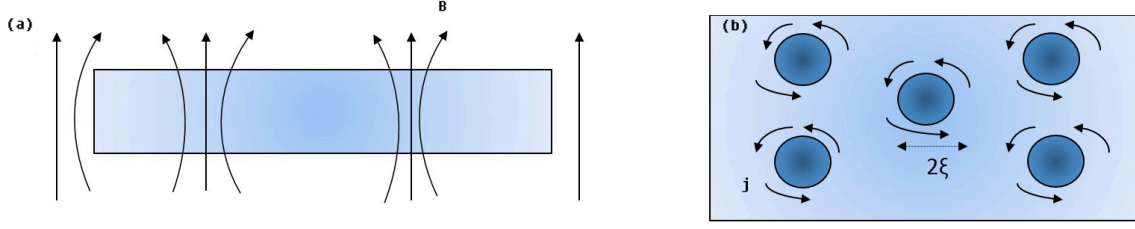
Figure 1.1: (a) Side view of the vortices. The lines represent the magnetic fields; (b) Top view. The current directions are shown. 2ξ is the estimated size of one vortex.

and comparing Eq. 1.27 with the definitions of λ(Eq. 1.19), ξ(Eq. 1.14) and B_c(Eq. 1.9), it's not difficult to get

$$B_{c2} = \sqrt{2}\kappa B_c. \tag{1.29}$$

This indicates that the value $\kappa = 1/\sqrt{2}$ classifies superconductors into two types: for $\kappa < 1/\sqrt{2}$ then $B_c > B_{c2}$, it's a type I superconductor; for $\kappa > 1/\sqrt{2}$ then $B_c < B_{c2}$, it's a type II. In the type II superconductors, when $B_c < B < B_{c2}$, the magnetic flux will penetrate into the superconductor in the form of vortex (Fig. 1.1). This state is called the mixed state and has been studied by many authors (check Ref. [39, 38] and the references therein).

1.3 BCS THEORY

The Ginzburg-Landau theory is a surprising success even though it's just a phenomenological theory. But it's impossible to fully understand the origin of superconductivity because the GL theory does not provide for any detail in the microscopic regime. To solve this, in 1957, Bardeen, Cooper, and Schrieffer (BCS) constructed a microscopic theory, referred to as the BCS theory, to explain and predict many properties of elemental superconductors [4]. And conversely, the GL theory found its microscopic base as it can be derived from the BCS theory [19].

The BCS theory evolved from the Cooper pair, which was proposed by Cooper [11] in 1956. In the Fermi sea, two electrons can form a bound state if they have

an attractive potential which can be very weak. That bound state will have a lower energy, below the Fermi sea ground state. In 1950, Fröhlich [14] pointed out that the attractive potential may originate from interactions between electrons and atom lattices. The lattice will be pulled toward the passing electron. When another electron passes the same position, it will be attracted by the displacing lattice. In this process, the two electrons can exchange a phonon through the lattice. This interaction was confirmed by the proportionality of T_c and H_c to $M^{-1/2}$ for isotopes of element superconductors, known as the isotope effect. This also suggests we can describe
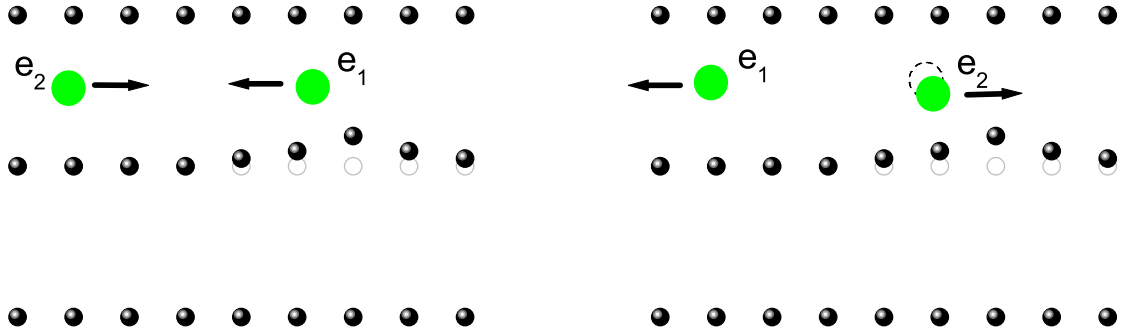
Figure 1.2: Pair attraction mediated by lattice. The electron 1 induces a distortion in the atom lattice. When the electron 2 passes by that distortion, its state is affected.

this pair model by a wavefunction

$$\psi_0(\mathbf{r}_1, \mathbf{r}_2) = \sum_{\mathbf{k}} g_{\mathbf{k}} e^{i\mathbf{k}\cdot(\mathbf{r}_1-\mathbf{r}_2)}\chi(1,2) \tag{1.30}$$

where $\chi(1,2)$ is the spin coupling function. It can be an antisymmetric singlet spin function $(\uparrow\downarrow - \downarrow\uparrow)$ or one of the symmetric triplet spin functions $(\uparrow\uparrow, \uparrow\downarrow + \downarrow\uparrow, \downarrow\downarrow)$. In our case , singlet coupling is expected to provide lower energy because it restricts the orbit function to be a sum of products of $\cos \mathbf{k}\cdot(\mathbf{r}_1 - \mathbf{r}_2)$ which will have a larger probability amplitude for the electrons to be near each other. Thus, the dominating

11

part of the wave function is

$$\psi_0(\mathbf{r}_1 - \mathbf{r}_2) = [\sum_{\mathbf{k} > \mathbf{k_F}} g_{\mathbf{k}} \cos \mathbf{k} \cdot (\mathbf{r}_1 - \mathbf{r}_2)](\uparrow\downarrow - \downarrow\uparrow) \tag{1.31}$$

By introducing the language of second quantization and including the background of Fermi sea, BCS chose the ground state as

$$|\psi_G\rangle = \Pi_{\mathbf{k}=\mathbf{k}_1,\ldots,\mathbf{k}_M}(u_{\mathbf{k}} + v_{\mathbf{k}} c^*_{\mathbf{k}\uparrow} c^*_{-\mathbf{k}\downarrow})|\psi_0\rangle \tag{1.32}$$

where $|v_{\mathbf{k}}|^2$ is the probability of the pair $(\mathbf{k}\uparrow, -\mathbf{k}\downarrow)$ being occupied and $|u_{\mathbf{k}}|^2$, which equals $1 - |v_{\mathbf{k}}|^2$, is the probability of being unoccupied. $c^*_{\mathbf{k}\uparrow}$ is the creation operator that creates an electron of momentum $\mathbf{k}$ and spin up, while its opposite, annihilation operator $c_{\mathbf{k}\uparrow}$, will annihilate an electron with same momentum and spin.

Only considering the attraction between the pair of electrons, we can write the hamiltonian as

$$H = \sum_{\mathbf{k}\sigma} \epsilon_{\mathbf{k}} c^*_{\mathbf{k}\sigma} c_{\mathbf{k}\sigma} + \sum_{\mathbf{kl}} V_{\mathbf{kl}} c^*_{\mathbf{k}\uparrow} c^*_{-\mathbf{k}\downarrow} c_{\mathbf{l}\uparrow} c_{-\mathbf{l}\downarrow} \tag{1.33}$$

where $\epsilon_{\mathbf{k}}$ represents the kinetic energy of the electron. As the derivation in [57], for the case with small fluctuations about the expectation $b_{\mathbf{k}} \equiv \langle c_{-\mathbf{l}\downarrow} c_{\mathbf{l}\uparrow}\rangle$, we reform the hamiltonian to be

$$H = \sum_{\mathbf{k}\sigma} \epsilon_{\mathbf{k}} c^*_{\mathbf{k}\sigma} c_{\mathbf{k}\sigma} + \sum_{\mathbf{kl}} V_{\mathbf{kl}}(c^*_{\mathbf{k}\uparrow} c^*_{-\mathbf{k}\downarrow} b_{\mathbf{l}} + b^*_{\mathbf{k}} c_{\mathbf{l}\uparrow} c_{-\mathbf{l}\downarrow} - b^*_{\mathbf{k}} b_{\mathbf{l}}) \tag{1.34}$$

Substitute the definition

$$\Delta_{\mathbf{k}} = -\sum_{\mathbf{l}} V_{\mathbf{kl}} b_{\mathbf{l}} \tag{1.35}$$

and the transformation [6]

$$c_{\mathbf{k}\uparrow} = u^*_{\mathbf{k}} \phi_{\mathbf{k}} + v_{\mathbf{k}} \phi^*_{-\mathbf{k}}$$

$$c^*_{-\mathbf{k}\downarrow} = -v^*_{\mathbf{k}} \phi_{\mathbf{k}} + u_{\mathbf{k}} \phi^*_{-\mathbf{k}} \tag{1.36}$$

into the hamiltonian, we have

$$H = \sum_{\mathbf{k}} \epsilon_{\mathbf{k}}[(|u_{\mathbf{k}}|^2 - |v_{\mathbf{k}}|^2)(\phi^*_{\mathbf{k}} \phi_{\mathbf{k}} + \phi^*_{-\mathbf{k}} \phi_{-\mathbf{k}}) + 2|v_{\mathbf{k}}|^2 + 2u^*_{\mathbf{k}} v^*_{\mathbf{k}} \phi_{-\mathbf{k}} \phi_{\mathbf{k}}$$

$$+ 2u_{\mathbf{k}} v_{\mathbf{k}} \phi^*_{\mathbf{k}} \phi^*_{-\mathbf{k}}] + \sum_{\mathbf{k}}[(\Delta_{\mathbf{k}} u_{\mathbf{k}} v^*_{\mathbf{k}} + \Delta^*_{\mathbf{k}} u^*_{\mathbf{k}} v_{\mathbf{k}})(\phi^*_{\mathbf{k}} \phi_{\mathbf{k}} + \phi^*_{-\mathbf{k}} \phi_{-\mathbf{k}} - 1) \tag{1.37}$$

$$+ (\Delta_{\mathbf{k}} v^{*2}_{\mathbf{k}} - \Delta^*_{\mathbf{k}} u^{*2}_{\mathbf{k}})\phi_{-\mathbf{k}} \phi_{\mathbf{k}} + (\Delta^*_{\mathbf{k}} v^2_{\mathbf{k}} - \Delta_{\mathbf{k}} u^2_{\mathbf{k}})\phi^*_{\mathbf{k}} \phi^*_{-\mathbf{k}} + \Delta_{\mathbf{k}} b^*_{\mathbf{k}}]$$

where $\phi_{\mathbf{k}}$ is similar to $c_{\mathbf{k}\uparrow}$. $\phi_{\mathbf{k}}$ destroys an electron with $\mathbf{k}\uparrow$ or creates one with $-\mathbf{k}\downarrow$. To eliminate the crossing terms $\phi_{\mathbf{k}}\phi_{-\mathbf{k}}$ and $\phi_{\mathbf{k}}^*\phi_{-\mathbf{k}}^*$, we can choose $u_{\mathbf{k}}$ and $v_{\mathbf{k}}$ to satisfy the following condition,

$$2\epsilon_{\mathbf{k}}u_{\mathbf{k}}v_{\mathbf{k}} + \Delta_{\mathbf{k}}^*v_{\mathbf{k}}^2 - \Delta_{\mathbf{k}}u_{\mathbf{k}}^2 = 0 \tag{1.38}$$

This has a solution as

$$\frac{\Delta_{\mathbf{k}}^*v_{\mathbf{k}}}{u_{\mathbf{k}}} = \sqrt{\epsilon_{\mathbf{k}}^2 + |\Delta_{\mathbf{k}}|^2} - \epsilon_{\mathbf{k}} \tag{1.39}$$

Define the excitation energy as

$$E_{\mathbf{k}} = \sqrt{\epsilon_{\mathbf{k}}^2 + |\Delta_{\mathbf{k}}|^2} \tag{1.40}$$

and combine with the requirement $|u_{\mathbf{k}}|^2 + |v_{\mathbf{k}}|^2 = 1$, we can have the exact values of $u_{\mathbf{k}}$ and $v_{\mathbf{k}}$,

$$\begin{aligned} |u_{\mathbf{k}}|^2 &= \frac{1}{2}\left(1 + \frac{\epsilon_{\mathbf{k}}}{E_{\mathbf{k}}}\right) \\ |v_{\mathbf{k}}|^2 &= \frac{1}{2}\left(1 - \frac{\epsilon_{\mathbf{k}}}{E_{\mathbf{k}}}\right) \end{aligned} \tag{1.41}$$

Now, return to the definition of $\Delta_{\mathbf{k}}$ and insert the Eq. 1.36 into it

$$\Delta_{\mathbf{k}} = -\sum_{\mathbf{l}} V_{\mathbf{kl}}u_{\mathbf{l}}^*v_{\mathbf{l}}\langle 1 - \phi_{\mathbf{k}}^*\phi_{\mathbf{k}} - \phi_{-\mathbf{k}}^*\phi_{-\mathbf{k}}\rangle \tag{1.42}$$

here the off-diagonal terms are ignored since they don't contribute to the averages. Since $\phi_{\mathbf{k}}^*\phi_{\mathbf{k}}$ and $\phi_{-\mathbf{k}}^*\phi_{-\mathbf{k}}$ are just number operators of excited fermi quasi-particles, their averages should both be equal to the usual Fermi function

$$f(E_{\mathbf{k}}) = \frac{1}{e^{\beta E_{\mathbf{k}}} + 1} \tag{1.43}$$

where $\beta = 1/kT$. Therefore, the BCS energy gap will be

$$\Delta_{\mathbf{k}} = -\sum_{\mathbf{l}} V_{\mathbf{kl}}u_{\mathbf{l}}^*v_{\mathbf{l}}[1 - 2f(E_{\mathbf{l}})] = -\sum_{\mathbf{l}} V_{\mathbf{kl}}\Delta_{\mathbf{l}}\frac{\tanh \beta E_{\mathbf{l}}/2}{2E_{\mathbf{l}}} \tag{1.44}$$

The BCS approximation, that makes $V_{\mathbf{kl}} = -V$ and therefore $\Delta_{\mathbf{k}} = \Delta$, is appropriate for the isotropic(s-wave) superconductors. The above equation for s-wave will turn out to be

$$\frac{1}{V} = \sum_{\mathbf{k}} \frac{\tanh \beta E_{\mathbf{k}}/2}{2E_{\mathbf{k}}} \tag{1.45}$$

13

and its integral form,

$$\frac{1}{N(0)V} = \int_0^{\hbar\omega_c} \frac{\tanh\frac{1}{2}\beta\sqrt{\epsilon^2 + \Delta^2}}{\sqrt{\epsilon^2 + \Delta^2}} d\epsilon, \tag{1.46}$$

where $N(0)$ is the density of electrons at the Fermi surface. From this equation, $\Delta(T)$ can only be calculated numerically. But it's easy to get its value at $T = T_c$ and $T = 0$. When $T = T_c$, $\Delta = 0$. Eq. 1.46 becomes [57]

$$\frac{1}{N(0)V} = \int_0^{\beta_c\hbar\omega_c/2} \frac{\tanh x}{x} dx = \ln 2e^\gamma \beta_c\hbar\omega_c/\pi \tag{1.47}$$

where γ is Euler's constant 0.577.... The above equation defines T_c as

$$kT_c = 1.13\hbar\omega_c e^{-1/N(0)V}. \tag{1.48}$$

When $T = 0$, Eq. 1.46 turns out to be

$$\frac{1}{N(0)V} = \int_0^{\hbar\omega_c} \frac{1}{\sqrt{\epsilon^2 + \Delta^2(0)}} d\epsilon = \int_0^{\hbar\omega_c/\Delta(0)} \frac{1}{\sqrt{1 + x^2}} dx. \tag{1.49}$$

This integral yields $arcsinh(\hbar\omega_c/\Delta(0))$. In the weak coupling limit $N(0)V \ll 1$, Eq. 1.49 gives

$$\Delta(0) = \frac{\hbar\omega_c}{\sinh(1/N(0)V)} \approx 2\hbar\omega_c e^{-1/N(0)V} = 1.764kT_c, \tag{1.50}$$

where Eq. 1.48 has been used.

For arbitrary T, people usually use the following approximate solution

$$\frac{\Delta(t)}{\Delta(0)} \approx 1.74\sqrt{1 - t} \tag{1.51}$$

as T gets close to T_c. We also found this expression

$$\frac{\Delta(t)}{\Delta(0)} \approx \tanh\frac{\sqrt{1 - t}}{\gamma t^{\pi/5}} \tag{1.52}$$

can fit the weak-coupling limit solution very well (Fig. 1.4).
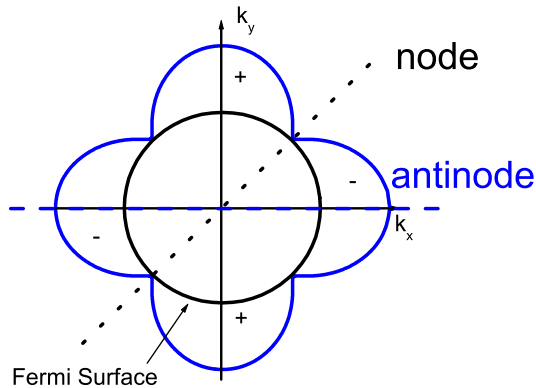
Figure 1.3: Schematic plot of the d-wave gap

d-wave superconductors

For simplicity, we assumed the energy gap $\Delta_{\mathbf{k}}$ was independent of the momentum $\mathbf{k}$, and this assumption is often referred to as s-wave pairing. However, not all superconductors have that simple relation. In superconductors like YBCO, $\Delta_{\mathbf{k}}$ will be dependent on $\mathbf{k}$, and its dependence is up to the crystal symmetry.

In d-wave ($\mathrm{d}_{x^2-y^2}$) superconductors, Δ—$\mathbf{k}$ dependence will be $\Delta_{\mathbf{k}} = \Delta\cos(2\phi)$ where ϕ is the angle of the quasiparticle momentum, which lies in the ab plane and starts from the a-axis. Hence it has four nodes at the Fermi surface (Fig. 1.3) [53] and an intrinsic phase shift by π in the antinode directions [54]. The latter property has been confirmed by the corner Josephson junction experiment [63, 62, 22]. Within the weak-coupling model, the temperature dependence of the d-wave Δ can be calculated by the following equation [64]

$$-\ln(\frac{\Delta(T)}{\Delta(0)}) =$$
$$\frac{8}{\pi}\int_0^\infty dx(1+e^{\beta\Delta x})^{-1}\{\theta(x-1)x[K(x^{-1})-E(x^{-1})]+\theta(1-x)[K(x)-E(x)]\}. \tag{1.53}$$

Where $K(x)$ and $E(x)$ are the complete elliptic integrals. Here $\Delta(0) = 2.14kT_c$ as
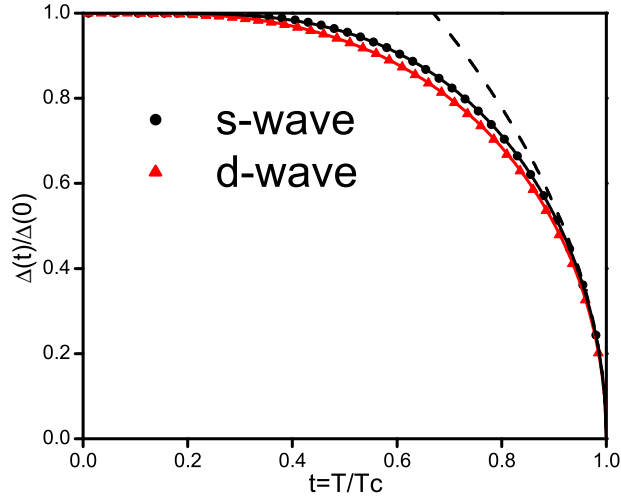
Figure 1.4: Temperature dependence of Δ for s-wave and d-wave superconductors. The solid curves are Eq. 1.52 and Eq. 1.54, respectively. The dashed line is Eq. 1.51.

in [64]. Like the s-wave equation, Eq. 1.53 can be only numerically solved, but its asymptotic solution is similar to Eq. 1.52, as

$$\frac{\Delta(t)}{\Delta(0)} \approx \tanh \frac{\sqrt{1-t}}{\frac{3}{5}t^{\pi/6}}. \tag{1.54}$$

Numerical calculations of the energy gaps

In Fig. 1.4, we calculated the energy gaps of s-wave and d-wave superconductors by the programs in Appendix A and compared them with Eq. 1.52 and Eq. 1.54, respectively. The relative errors of these two fittings are both $< 1\%$ in the whole temperature range. These equations can be useful for the calculations of other quantities which depend on the energy gaps.

16

DEPAIRING CURRENT DENSITY IN SUPERCONDUCTORS

The depairing current density is that at which the kinetic energy of the superconducting carriers equals the binding energy of the Cooper pair, and hence is the current threshold above which the superconductivity of the superconductor is totally destroyed and the superconducting energy gap Δ vanishes. The depairing (or pair-breaking) critical current density j_d represents — along with the critical temperature T_c and the upper critical field B_{c2} — one of the intrinsic critical parameters that sets a fundamental limit to the survival of superconductivity. While T_c and B_{c2} are measured routinely, j_d is seldom measured because of technical difficulties associated with sample heating at high currents.

A series of useful reviews [3, 13, 32] have been given on the calculation of the depairing current. These theoretical calculations cover different regimes. The simple London equations are valid at T_c, but it failed at the lower temperature since it did not take into account the effect of the change in the order parameter with the current. The GL theory gives a good phenomenological treatment that works well close to T_c. For low temperatures, some other theories based on the microscopic theories were proposed.

2.1 DEPAIRING CURRENT DENSITY IN LONDON EQUATIONS FRAMEWORK

j_d can be roughly estimated from the London equations by equating the kinetic energy to the free energy density,

$$\frac{1}{2}n_s m^* v_s^2 = \frac{B_c^2}{2\mu_0}.$$ (2.1)

17

Substituting $v_s = j_s/2en_s$ and Eq. 1.20 into the above equation, we have

$$j_d = \frac{B_c}{\mu_0 \lambda_L} \tag{2.2}$$

This simple derivation has assumed that n_s will not be affected by j approaching j_d. This is far from reality, but gives an idea that j_d strongly depends on the critical field and the penetration depth.

2.2 DEPAIRING CURRENT DENSITY IN GINZBURG-LANDAU THEORY FRAMEWORK

From Eq. 1.16, we can define the velocity of the quasiparticle in a superconductor as

$$\mathbf{v}_s = \frac{\hbar}{m^*}(\nabla\varphi - \frac{2\pi}{\Phi_0}\mathbf{A}). \tag{2.3}$$

Substitute this into Eq. 1.16 and Eq. 1.12, we have

$$\mathbf{j} = 2e\psi_0^2\mathbf{v}_s, \tag{2.4}$$

and

$$a + b\psi_0^2 + \frac{1}{2}m^*v_s^2 = 0. \tag{2.5}$$

Then the optimum value of ψ_0 for the minimization of the free energy is given as

$$\psi_0^2 = \frac{|a|}{b}(1 - \frac{m^*v_s^2}{2|a|}) = |\psi_m|^2[1 - (\frac{\xi m^* v_s}{\hbar})^2]. \tag{2.6}$$

Putting this into Eq. 2.4, we arrive

$$j = 2e|\psi_m|^2[1 - (\frac{\xi m^* v_s}{\hbar})^2]v_s. \tag{2.7}$$

When $\frac{\partial j}{\partial v_s} = 0$, which gives $v_s = \hbar/\sqrt{3}m^*\xi$, the current reaches its maximum. Thus, the depairing current is

$$j_d = \frac{4e|\psi_m|^2\hbar}{3\sqrt{3}m^*\xi}. \tag{2.8}$$

Combining this with the London penetration depth, we finally get

$$j_d = \frac{\hbar}{3\sqrt{3}\mu_0 e\lambda_L^2\xi} = \frac{\Phi_0}{3\sqrt{3}\pi\mu_0\lambda_L^2(T)\xi(T)}. \tag{2.9}$$

With the empirical temperature dependence $\lambda_L(t) = \lambda_L(0)/\sqrt{1-t^4}$ and $\xi(t) = \xi(0)/\sqrt{1-t}$ near T_c, the transition temperature shifts lower with a $j^{2/3}$ proportionality:

$$1 - \frac{T_c(j)}{T_c(0)} \approx \left(\frac{1}{4}\right)^{\frac{2}{3}} \left[\frac{j}{j_d(0)}\right]^{\frac{2}{3}} \tag{2.10}$$

with

$$j_d(0) = \sqrt{\frac{2\Phi_0}{27\pi\mu_0^2}} \left(\frac{\sqrt{B_{c2}(0)}}{\lambda_L^2(0)}\right), \tag{2.11}$$

where $B_{c2}(0) = \Phi_0/2\pi\xi(0)^2$ is defined as the upper critical field at zero temperature. In MKSA units, Eq. 2.11 becomes

$$j_d(0) = 5.56 \times 10^{-3} \times \sqrt{B_{c2}(0)}/\lambda^2(0), \tag{2.12}$$

where j_d is in A/m^2, B_{c2} is in Teslas and λ is in meters. In this formula, we took off the subscript of λ_L to prevent confusion. Note that if heat removal from the sample is ineffective, Joule heating will give an apparent shift $\Delta T_c \propto \rho j^2$, which is the cube of the intrinsic $\sim j^{2/3}$ depairing shift near T_c.

2.3 Depairing current density from the quasiparticle energy shift

At low temperatures, the quasiparticle drift will shift its energy by $\hbar k_F v_s$ where k_F is the wavevector at the Fermi surface. Thus, the gap vanishes when [3]

$$v_s = v_\Delta = \frac{\Delta}{\hbar k_F} = \frac{\Delta}{m v_F} \tag{2.13}$$

where m is the mass of one electron. Rewrite Eq. 2.7 as

$$j = 2en_s[1 - (\frac{v_s}{v_o})^2]v_s \tag{2.14}$$

where $v_o = \hbar/m^*\xi$. Since v_o is the maximum velocity of quasiparticles in GL's framework, it's reasonable to compare it with v_Δ. This gives a characteristic length related to Δ and the ratio of electron mass to the effective mass

$$\xi_\Delta = \frac{\hbar v_F}{\Delta}(\frac{m}{m^*}). \tag{2.15}$$

19

Eq. 2.15 is similar to the definition $\xi_0 = \hbar v_F / \pi \Delta(0)$ [57] at zero temperature.

For $v_s \ll v_\Delta$, $j = 2en_sv_s$ is strictly proportional to the density of quasiparticles n_s and the velocity. When it's close to T_c, the density is proportional to the order parameter $|\psi|^2$ in GL and then the temperature dependence $j^{2/3} \propto \Delta T_c$ is recovered. But at low temperatures, a more microscopic calculation is required to take into account the effect of the modification on the quasiparticle density by the drifting velocity.

2.4 MICROSCOPIC THEORY OF DEPAIRING CURRENT DENSITY

A number of authors have calculated j_d based on microscopic equations [3, 42, 47, 41]. These derivations usually started from the Gorkov equations or its simplified version, the Eilenberger equations. All of these calculations are out of the scope of our discussion here. But it's interesting to notice that, in Ref. [50] the authors found that the result of Kupriyanov and Lukichev(KL) [41] is close to the phenomenological expression

$$j_d = \frac{j_d(0)}{2\sqrt{2}}(1 - t^2)^{3/2}, \tag{2.16}$$

that was suggested by Bardeen [3] in the dirty limit, which actually is Eq. 2.2. Eq. 2.16 can also be derived from the formalism of the Eliashberg theory [45]. And it's also important to point out that the predictions on the temperature dependence of j_d from these microscopic theories are as same as GL theory's when the temperature is near T_c. In Fig. 2.1, the results of different theories are compared.

2.5 PREVIOUS EXPERIMENTAL WORK ON DEPAIRING CURRENT DENSITY

High current pulses are frequently used to probe depairing current densities in superconductors because short pulses can reduce the self heating effect and heat generation at the contacts. In Ref. [30, 34], single-shot square pulses with duration $\sim 2\mu s$ were sent to the YBCO and MgB$_2$ samples showing that the depairing current densities of
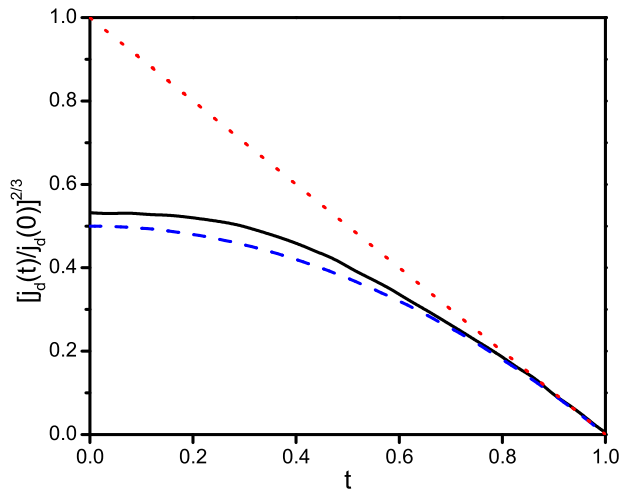
Figure 2.1: Temperature dependence of j_d from different theories. Replotted from Ref. [41]. The solid curve is KL theory, the dashed one is Eq. 2.16 and the dot one is GL's result.

these two materials were in agreement with the GL theory. In some systems, short pulses cannot completely exclude the sample heating. For example, a 50ns short high-current-pulse still generated significant amount of heat in a YBCO sample [35].

Aside from the single-shot square pulses, some authors used current pulses with a growing amplitude to measure the depairing current densities of superconducting films, Nb and a-MoGe [51] and $Nb/Pd_{81}Ni_{19}$ bilayers [10]. The duration of the pulse they used was $3 \sim 5ms$, which is much longer than the usual square pulse. Hence their results showed a noticeable change in temperatures due to the heating of high currents. The results of the depairing current densities of Nb, a-MoGe and $Nb/Pd_{81}Ni_{19}$ bilayers could be fit by the KL theory.

Generally, it is difficult to reach the value of $j_d(0)$ in YBCO because it is on the order of 10^8 A/cm^2. However, Arpaia *et al.* showed that it is possible for a YBCO nanowire with a protecting gold capping layer [2]. They measured multiple YBCO bridges with cross sections as small as 50×50nm^2. The ones covered by Au capping layers allowed them to get very high current densities which were up to 1×10^8 A/cm^2

21

at 4.2K. They also found the measured values of j_d conformed the prediction of the GL theory.

In the present work, we studied the n-type cuprate superconductors SLCO and NCCO, which had never been tested in the regime of current induced pair-breaking, by single-shot square pulses to examine the depairing mechanism in these superconductors. The techniques we used are similar to that in Ref. [34] but with a big improvement in the temperature control implemented by a sound trigger system which is discussed in Chap. 4. Valuable information was learned about the superfluid density as well as the penetration depth, which in the case of NCCO can not be obtained through magnetization measurements.

CHAPTER 3

CUPRATE SUPERCONDUCTORS

High temperature superconductors are very important, as some of them only require liquid N_2. This ease of use allows for many more applications. However, the theory of cuprate superconductors still remains a major challenge in current research. The BCS or GL theory is able to interpret partial properties of high-temperature super-conductivity. But, due to the the extreme anisotropy induced by the crystalline, both the BCS and GL theories need a big change, or we may need a complete new starting theory to fully understand the high temperature superconductivity.

3.1 CRYSTALLINE STRUCTURE OF CUPRATE SUPERCONDUCTORS

Even though the theory is still not clear, the copper oxide (CuO_2) planes in cuprate superconductors are believed to dominate the properties since all of those systems own similar CuO_2 planes [12]. Between the planes, the charge reservoirs control the oxidation state of adjacent superconducting planes and contribute either holes or electrons to the cuprate planes. In Fig. 3.1, the crystals of three cuprate superconductors, $Sr_{1-x}La_xCuO_2$ (SLCO), $Nd_{2-x}Ce_xCuO_4$ (NCCO) and $YBa_2Cu_3O_{7-x}$ (YBCO), are shown as examples. Their lattice parameters are listed in Table 3.1.

Table 3.1: The dimensions of one unit cell of cuprate compounds

Compound	a(Å)	b(Å)	c(Å)
SLCO [48]	3.952	3.952	3.389
NCCO [43]	3.94	3.94	12.1
YBCO	3.82	3.89	11.68
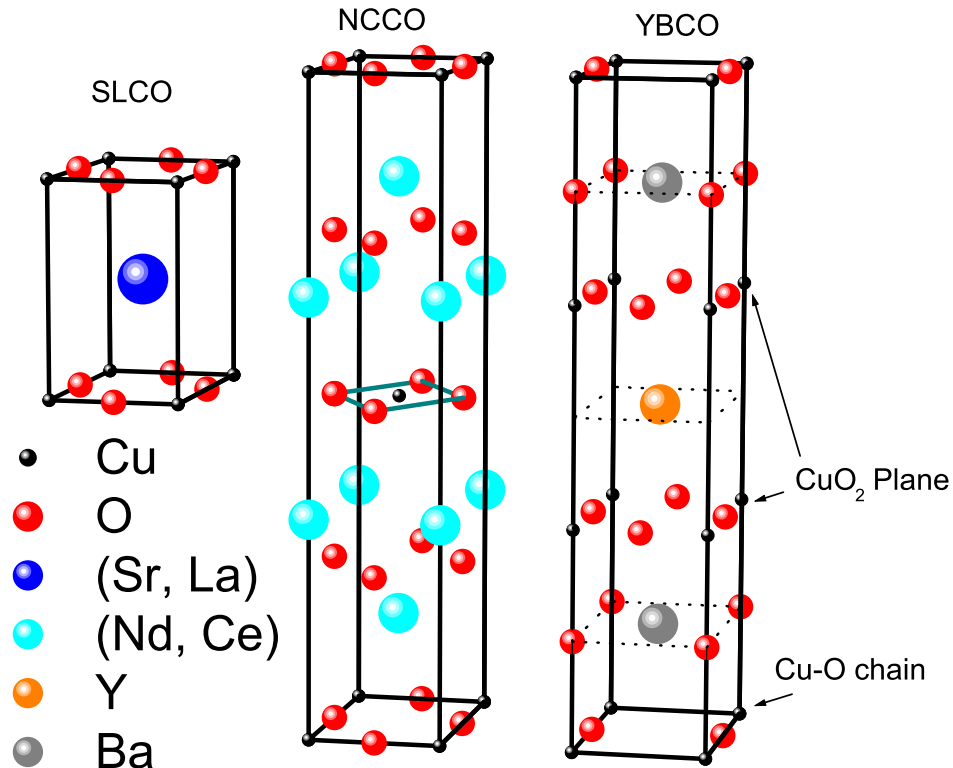
Figure 3.1: Crystalline structures of SLCO, NCCO and YBCO.

SLCO is an infinite-layer electron-doped superconductor [1]. The term "infinite-layer" implies that all of the atoms are not bound together by electrostatic bonding between discrete molecules, but rather by covalent or co-ionic bonding which makes a compound without a clear separation between molecules. This structure is most simple in all the cuprate superconductors but has a lot of difficulties in the sample preparation [27]. Its charge reservoir is just Sr ions. The doping element La has been assumed to have valence 3+ which is larger than Sr's 2+, which means SLCO is electron-doped.

As the first cuprate superconductor to exhibit n-type conduction, NCCO is single-layer cuprate compound. Its structure is a body-centered tetragonal, which is much more complicated than SLCO. In this compound, the neodymium has a valence 3+

and in the doping, Ce^{4+} takes its place.

In YBCO, two CuO_2 planes in one unit shell are separated by the yttrium atoms. The distance between them is about ~ 3.2 Å. The charge reservoirs between these pairs of planes contains barium, copper and oxygen. Some of the copper and oxygen atoms form CuO chains. These chains are perfect when the concentration of the oxygens is maximum, i.e. $x = 0$. Increasing x will introduce defects into the chains. No chain exists in the case of the undoped compound when $x = 1$. Because of the excess oxygens, YBCO is a hole-doped superconductor.

3.2 ELECTRONIC STRUCTURE

In the undoped parent compound of cuprate superconductors, the Cu atom has a d^9 electronic configuration. But, due to the Jahn-Teller effect, the highest occupied orbital in Cu is $d_{x^2-y^2}$ which is split from the degenerate orbital e_g of d^9. The $d_{x^2-y^2}$ orbital will strongly couple with the oxygen p_x, p_y orbitals to form a covalent bond. These half-filled hybridization states and strong localization result in an antiferromagnetic (AFM) Mott insulator. A full review of theories on how to describe the electronic models in cuprate superconductors has been given by Dagotto [12]. Here we focus on SLCO which has a special structure.

In the discussion by Wang *et al.* [60] using the first-principles calculations, the electronic structure also shows $d_{x^2-y^2}$ symmetry when the $SrCuO_2$ crystal is perfect. But if the O atoms are shifted out of the CuO_2 planes, the p_y orbital of the oxygen will hybridize with d_{xy} from Cu more than with $d_{x^2-y^2}$. This results in an antibonding state with π-character. So the nodes of the superconducting gap are pushed below the Fermi level and the gap becomes nodeless. This π-bond character has been seen in the angle-resolved photoemission spectroscopy measurements conducted by Harter *et al.* [24]. An s-wave gap in SLCO was suggested by the quasiparticle tunneling spectra measurement [8]. However, the results of the muon spin spectroscopy measurement

that was done by Satoh *et al.* [52] showed that the gap in SLCO has d-wave symmetry. This contradictory issue needs future studies to clarify.

Chapter 4

Apparatus and Experimental Techniques

This chapter will discuss the experimental techniques we used.

4.1   Sample preparation

The superconducting films used in the experiments were provided by external collaborators. However the remaining patterning was done in our laboratory. A four-probe pattern is used in the measurements. In order to etch a pattern on a superconductor film, the first step is to prepare a microscope slide with uniform photoresist covering and expose the negative pattern on it by the projector-camera system. After a development, a thick film is deposited on the slide. Acetone is used to clean the remaining photoresist and the mask. Inserting this slide into the light path of the microscope, we can see the positive pattern in the microscope view. With this mask, the standard photolithography procedure plus ion milling or acid etching can be used to create a pattern on the superconductor film. A single bridge mask is used for NCCO and SLCO. But for an anisotropy measurement, we have to use a multi-bridge mask (Fig. 4.1) with all the bridges arranged in different directions. The pair of big electrodes (top-center pairs in the figure) serve as the voltage and current negative electrodes separately for all bridges. After the pattern is done, the wires are bond on the sample by indium.
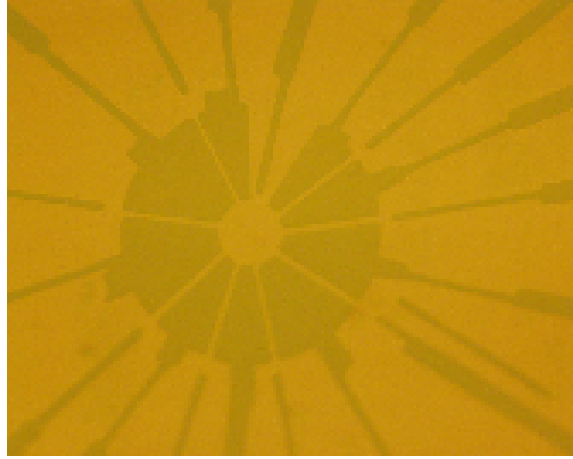
Figure 4.1: Anisotropic pattern on the YBCO film (covered by the photoresist as protection)

Spin processor

A spin coater WS-650SZ-6NPP/LITE from Laurell Technologies Corp 4.2 was used for the photoresist coating. The spinner is compact and packed with advanced features of automatic control, high-performance drive up to 12,000 RPM, and multi optional chucks etc.. It uses high pressure and dry air to drive the pneumatic vacuum generator and protect its motor.

Spinner Operation

1. Turn on the power supplies of the spinner and compressor.

2. Make sure the outlet pressure of the compressor is in the range of $60 \sim 70$psi.

3. Press "Select Process" and use the up-down buttons to choose the saved set up process or create a new one.

4. Press "Edit Mode". Check all the settings. If you want to modify, press "tab <" and then move the flashing cursor to choose the parameter to change.

5. Press "Run Mode" and confirm the settings.

Figure 4.2: Spin coater machine.

6. Open the lid and mount a right vacuum chuck. The 3mm chuck is a good choice for a small sample. For a slide, the specific chuck should be used.

7. Put the sample or slide on top of the chuck with carefully aligning the center of the sample at the axial of the chuck.

8. Press "Vacuum". The Vac reading on the screen should rise from 0 to about 23. If not, check the compressor and the contact between the chuck and sample. If the O-ring of the chuck is leaking, replace it.

9. Drip the photoresist or other chemicals on the top of the sample. Make certain that the chemical covers the whole surface without any bubbles. None of the chemicals should get into the hole of the chuck. If that happens, it may damage the motor. Therefore, it's very important to confirm the vacuum in the last step to make sure the seal is good.

10. Close the lid.

11. Confirm the LED of the "Start" button is illuminating.

12. Press "Start". The chuck will start rotating. Wait for it to finish. If something goes wrong, press "Stop".

13. After it stops, open the lid.

14. Press "Vacuum". The Vac reading drops down to 0.

15. Take out the sample.

16. If finished all the coating, put a protecting cap on the chuck and close the lid. Turn off the power supply and the compressor.

Mask exposure system

A projector-camera system is designed to expose a large pattern on the microscope slide. As presented in Fig. 4.3, a projector is aligned coaxially with a camera. When the projector is on, the image from a computer will be projected into the camera and it will expose the film that is replaced by a photoresist-covered slide. The size of a pattern on the slide can be as large as $1.5cm$ in diameter(Fig. 4.4).

Procedure to expose a mask

The whole procedure should be in a dark room or under a yellow light.

1. Create a negative pattern PowerPoint slide on a computer with white color for the pattern and dark for the rest.

2. Clean a microscope slide very carefully and spin photoresist on it for 50s at 3000rpm.

3. Mount the camera on the holder and put the projector under the camera with the lens face to the camera lens. Connect the projector to the computer in a slide show mode.
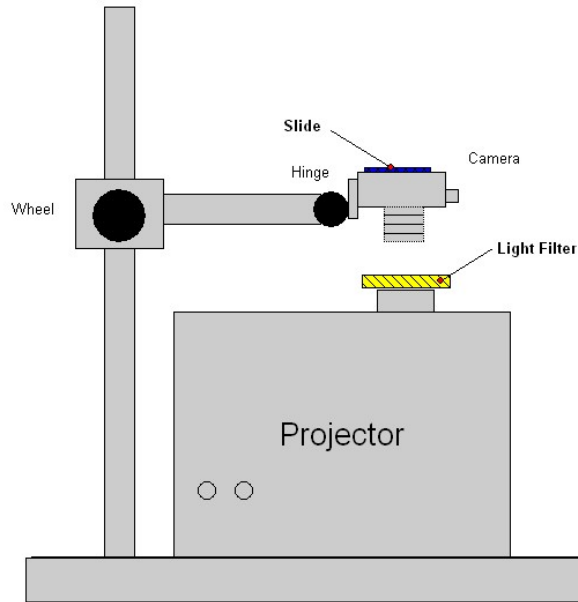
Figure 4.3: Projector-camera mask exposure system
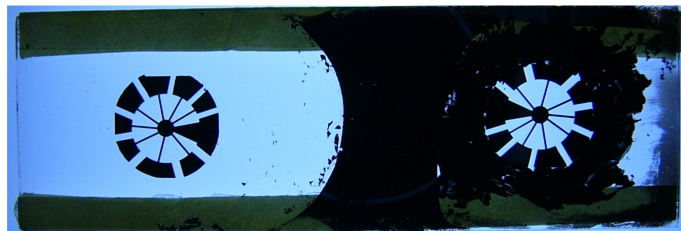
Figure 4.4: The masks for the anisotropy measurement. Two on one slide. Right hand side one is chosen for use, hence the dark ink was put on around the pattern to block the light.

4. Set the lens of the camera to "focus at infinity". Put the slide into the film house of the camera with the slide holder (copper board with a hole on it).

5. Insert a yellow light filter on top of the lens of projector. Turn on the projector.

6. Keep the shutter of the camera open. Adjust the focus of the camera by the wheel of holder and also the angle by the hinge. Make the image on the slide as sharp as possible.

7. Close the shutter and remove the light filter. Set the camera exposure time to be 1s.

31

8. Click the shutter to expose the slide.

9. Put the light filter back. And turn off the projector. Take the slide to develop.

DC magnetron sputtering

After the development of photoresist following the mask exposure, a thick metal film should be deposited on the slide so that the mask is permanently on the slide. Here, we used a niobium target and DC magnetron sputtering system. Because the slide is large, two rounds of deposition are necessary to make the film uniform. The first round uses 50 W power and deposits for 10 minutes. Then take out the slide and rotate it for another $5 - 10$ minutes deposition.

The following operations were used in the deposition process and started from the point where the system was totally off that means all electronics are off and vacuum valve are at off position.

Vacuum preparation

1. Turn on the water for deposition system and cryogenic pump compressor cooling. Make sure it has enough water flow for the deposition system. If not, the interlock indicator of MDX1K power supply will be off and the sputtering gun will halt. In this case, adjust the water valve to increase the water flow.

2. Connect the power of the system and compressor.

3. Put the sample holder into the deposition chamber. Before close the lid, check if the o-ring is clean. Close the lid.

4. Turn on the rough pump and then open the cryo rough valve slowly.

5. Turn on the MKS 286 gauge. The reading of cryopump (channel 1) should drop off very fast. After it dropped out of the scale, wait more 15 minutes to proceed.

6. Close the cryopump rough valve. If the pressure rises beyond 50 micron psi, open the rough valve again. Repeat this serval times until the reading of channel 1 remains out of scale with rough valve off.

7. Turn on the cryopump compressor. Let the temperature of cryopump drop to approximately 10 K. This will take about 5 hours. Meanwhile, open the vacuum rough valve slowly and allow the rough pump to pump down the chamber. The reading of channel 2 of MKS 286 gauge should drop down. If not, check vacuum leak of the chamber. It's also recommended to turn on the band heater of the chamber at 65 V, that will heat up the chamber and help it to release the absorbed gas. Turn off the MKS 286 gauge.

8. After 5 hours, turn on the MKS 286 gauge to check the vacuum. Both channels should be out of scale now. If they are, turn the gauge off. If the band heater is on, also turn it off.

9. Close the chamber rough valve and open the high vacuum valve fully (21 and half turns in the counterclockwise direction). Let the cryogenic pump to run overnight (about 8 hours).

10. Turn on MKS 286 to confirm the bars of two channels are both at zero off scale. If not, check vacuum leak.

11. If MKS 286 shows correct values, turn on MKS 290 ion gauge to get the high vacuum pressure value. The gauge should read in the order of 10^{-6} torr. Then turn on the degas and allow the pressure to reach its minimum. Record the minimum value. Turn off degas and then the gauge.

The above steps give you the necessary vacuum for the deposition. Only if the system is in a high vacuum, the following deposition steps can be proceeded.

Deposition procedures
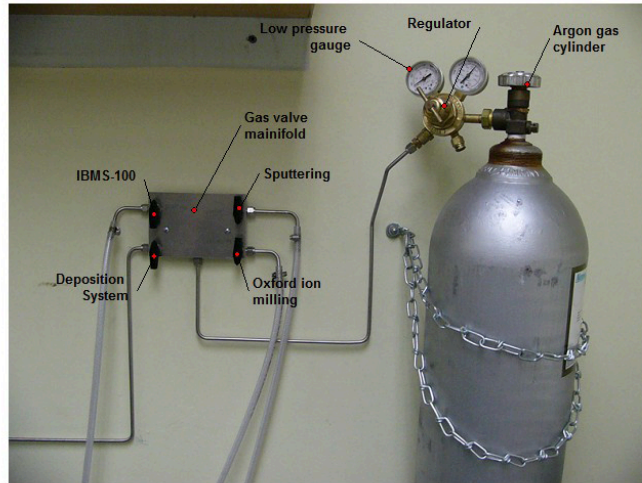
Figure 4.5: The manifold valves.

1. Turn on the MKS PDR-1C gauge and wait until its reading is less than 10×10^{-3} torr. This takes about half hour.

2. Rotate the high vacuum valve 17 and a half turns in the clockwise direction, i.e. just leave it open at 4 turns. It throttles the pumping speed and protects the cryopump.

3. Open the Argon cylinder and adjust the regulator to 10 psi. Switch the manifold valves to deposition system as in Fig. 4.5.

4. Open the gas bleed needle 4 turns and then turn slowly until the reading of MKS PDR-1C rises to 20×10^{-3}.

5. Turn on the power of MDX power supply. The interlock indicator should be lit. If not, check the water flow of the deposition system.

6. Set the power as required.

7. Turn on the DC switch on the front panel. The actual power of MDX rises up and neon can be seen inside the chamber through the viewport. Wait ~ 30s to let the plasma to clean the target.

8. Open the gun shutter and start the timer. Wait for the time as required.

9. Close the gun shutter.

10. Turn off the DC switch and close the gas bleed needle. Turn off the MKS PDR-1C gauge.

11. Close the high vacuum valve. And then vent the chamber.

12. Take out the sample holder out.

After one deposition, the chamber will be at atmospheric pressure. But if another round of deposition is needed, it's not necessary to start from zero. A warm start routing can save a lot of time since the cryopump is at about 10 K. Before any of the following steps, make sure the gas bleed needle is off and the manifold valves are all at off position.

Warm start routing

1. Turn on the rough pump valve.

2. Wait until the channel 2 of MKS 286 drops off scale.

3. Close the rough pump valve and then open the high vac valve fully. Let it pump about 20 minutes.

4. Use the MKS 290 to check the vacuum as above.

5. The system is ready for another deposition procedure.

If the system is expected in idle state for more than one day, make certain the high vac valve is closed and all the gauges are off. And when it's reused, follow the *warm start routing.*

To completely shut down the system, close all of the valves and turn off all devices. Then turn off the rough pump and cryopump compressor. Let the water flow another
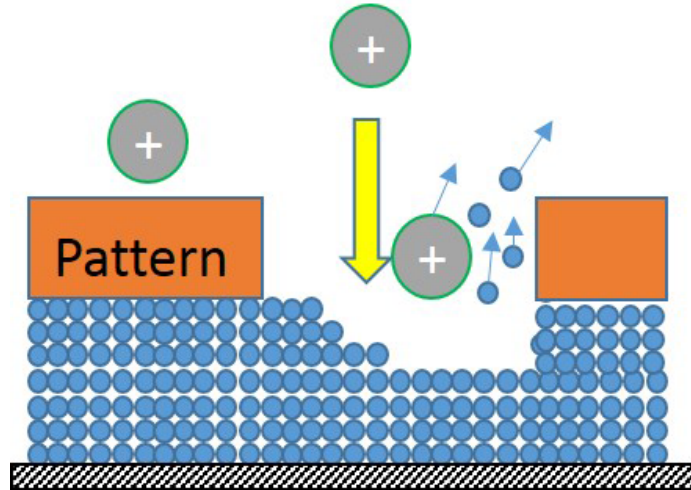
Figure 4.6: Ion milling. The ions (typically argon) accelerated by a high voltage bombard the film. The unprotected part of the film will be etched.

half hour to totally cool down the compressor and also the sputtering gun if it's used just a moment ago. Close the water.

Ion-milling system

Ion milling is used for etching a pattern onto a thin film (Fig. 4.6). This process is totally dry and clean. Therefore it's very good for materials that are sensitive to moisture, such as YBCO. We have two ion-milling systems: Oxford IG5 and TFS IBMS-100. Oxford IG5 uses a nozzle as an anode. Here, the nozzle is replaced by a homemade one which was modified from a piece of stainless steel 316 seamless round tubing with part number CTSXX-6205-24. The IBMS-100 system uses a 3cm ion source from Commonwealth Scientific Corp.

In the present experiments, we used the small Oxford IG5 which is connected to the big IBMS-100 ion milling system so that they can share the vacuum system (Fig. 4.7). When using IBMS-100, the inlet gas valve (the green knob) of Oxford IG5 must be fully closed or the gun head replaced with a flange cap.

Operation for Oxford ion gun
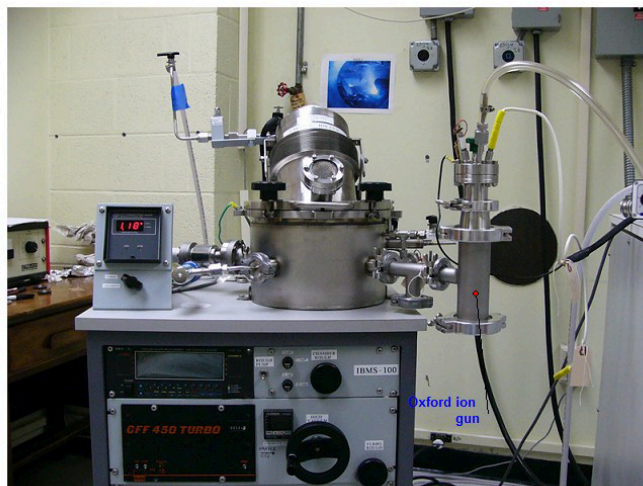
Figure 4.7: Oxford ion gun and IBMS-100

1. Make sure everything is at off position. The flow control valve should be at 0 and the green knob should be open. The lid of IBMS-100 should be also closed.

2. Carefully put the sample at the marked position inside the ion milling chamber. Mount the gun head with matching the marker positions at both ends.

3. Turn on the rough pump.

4. Open the turbo rough valve fully.

5. Switch the vacuum gauge to the turbo position and monitor it. Wait for it to drop under 20 mTorr.

6. Turn on the turbo pump. Push the switch to "ON" and it will return to middle. At first, the yellow LED is on. After about 2 minutes, the green one will be lit. That means the turbo pump is in a full speed. The turbo should be used only under the full speed.

7. Fully close the turbo rough. Pay attention here. The panel is not flat so the knob may touch the panel when it's closing. Go for one more turn when it has touched the panel.

8. Open the chamber rough and switch the vacuum gauge to the chamber position. Let it drop to under 100 mTorr.

9. Close the chamber rough and switch the vacuum gauge again back to the turbo position. Open the turbo rough again. Wait the reading drop back to 20 mTorr.

10. Check the chamber pressure and make sure it's less than 1000 mTorr. If not, make sure it's not leaking or repeat pumping the chamber by the rough pump with the turbo rough closed.

11. Slowly and carefully open the high vacuum valve while monitoring the vacuum of the turbo back end. It should not be over 100 mTorr.

12. Let it pump for about 20 minutes.

13. Open the argon gas cylinder and switch the manifold(Fig. 4.5) to old ion gun. Adjust the low pressure gauge to be 10 psi.

14. Set the flow control valve to be 6.1. Wait about 20 minutes to let the pressure to be stable.

15. Make sure only the beam probe has been connected to the gun head. The bias probe should not be connected. Turn on the power of the ion gun.

16. Adjust the beam current. The beam current should be able to reach $100\mu A$ with the beam energy less than 2.5keV. Never use a higher energy. It's normal if the current is less than the expected value at the beginning since it usually will rise after it is heated up. If it failed to reach $100\mu A$, check the pressure. Adjusting the high vacuum valve may be helpful.

17. When the ion milling is finished, turn off the ion gun power supply. Close the gas cylinder and the flow valve.

18. Close the high vacuum valve. Now it is ready to vent the chamber.

After the above procedures, the pump station is still on with the turbo pump at full speed, the turbo rough valve open and the following valves closed: chamber rough, high vacuum and flow control valve. To completely shut it down, the turbo pump should be turned off first and then the rough pump should run for another half hour to let the turbo pump slow down; it should also be cooled down by fan. Then close the turbo rough. It's ok to shut down the rough pump now.

But if it's necessary to take another ion milling soon, it's better to keep the turbo running. For one more ion milling, just start from Step 7.

4.2 Cryostats and magnet

Two Cryomech pulsed-tube closed-cycle refrigerators, PT405 and PT60, were set up in our laboratory. PT405 cryorefrigerator can cool down to < 4 K and the standard four-probe measurement wires for one bridge were set up on it. It was mainly used for measuring NCCO and SLCO samples that have a low T_c. And also this cryostat was installed with a GMW 3473-50 electromagnet(Fig. 4.8). It allows us to measure the H_{c2} of all the samples. Another refrigerator is PT60. Its capable of cooling is down to ~ 30 K. For this reason, it's only good for higher T_c superconductors. With PT60, we designed it to be able to measure 8 bridges on one superconductor sample simultaneously. Hence many more wires were mounted on PT60 than ones on PT405.

PT405 refrigerator

The detailed diagram of the PT405 cryostat and magnet is in Fig. 4.9. PT405 is a two stage pulse tube cryocooler. It works with a Cryomech CP950 compressor which requires water cooling to function. When it's running, the helium is compressed by the compressor and then expands in the cold head. The expansion first happens in the first station that will also cool down the gas and then in the second stage to bring
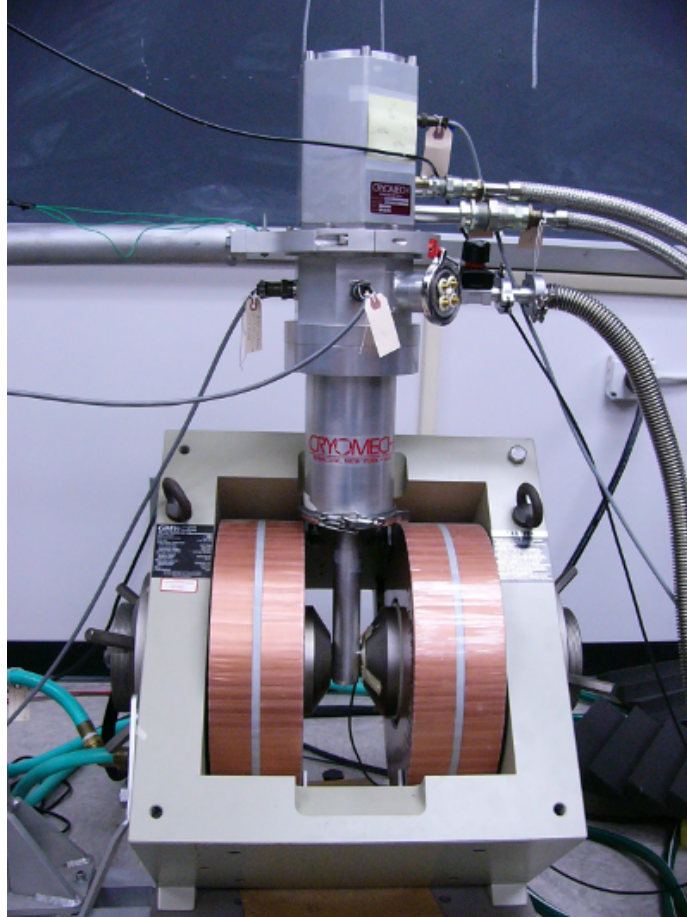
Figure 4.8: PT405 cryostat with GMW 3473-50 magnet.

the temperature lower. A two-stage cryocooler usually provides a lower temperature than a one-stage cryocooler, but the path of the gas running through will be longer and therefore the frequency of compression and expansion will be lower (~ 1.4Hz). This results in a fluctuation of the temperature. To get the temperature stable, we have to use the sound trigger system for PT405 as discussed in Sec. 4.3.

The water-cooled GMW 3473-50 magnet is installed on a rotor. It can be rotated horizontally. Two ferromagnetic iron cores can be pulled out while mounting the sample. The maximum field is about 1.1 T. One Hall magnetic sensor is placed on one of iron pole face to measure the field strength between the iron pole faces. The sample holder is on the end of an extensional copper rod from the second stage of the pulse tube. The holder is also in between the magnet poles so that the applied
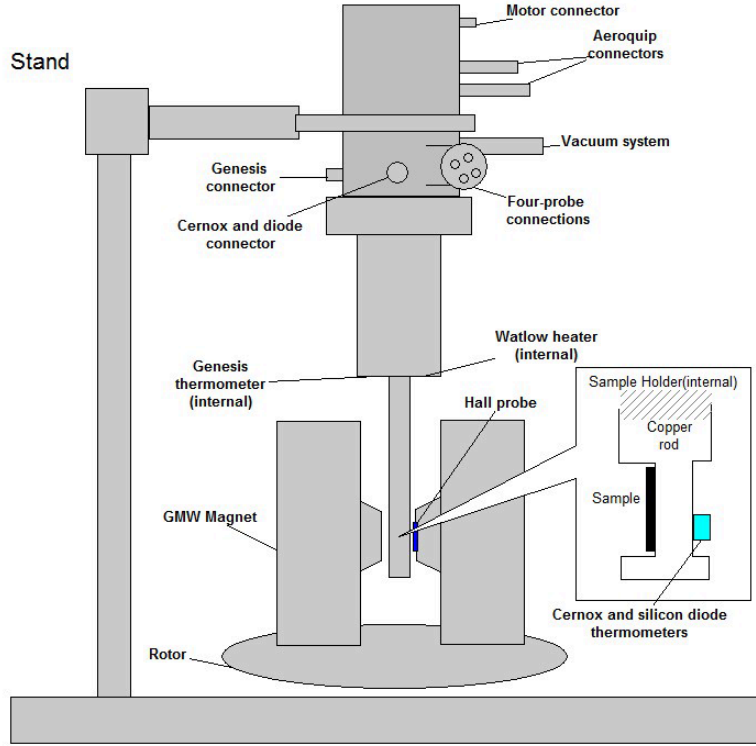
Figure 4.9: Schematic of PT405 and its magnet. The inset is the sample holder. The internal positions of sensors and heater are also present.

magnetic field on a superconductor sample can be adjusted.

PT60 refrigerator

PT60 is a single stage pulse tube cryocooler. Its cycling frequency is about twice of PT405's ($\sim$ 3Hz) that makes its temperature much more stable and hence it is not necessary to use the sound trigger system. A stack of two copper plates is mounted on the cooling stage(Fig. 4.10). The bottom one of that stack is not fixed but replaceable. By choosing different sizes of copper plates, we can adjust the cooling power from the cooling stage to the top copper plate. Our goal is to use a 50W heater to heat up the top plate and rise the temperature of the sample to 100K. To calculate the cross section of the bottom copper plate, we start from the heat conduction formula

$$q = -k(T_1 - T_0)/d \tag{4.1}$$

41
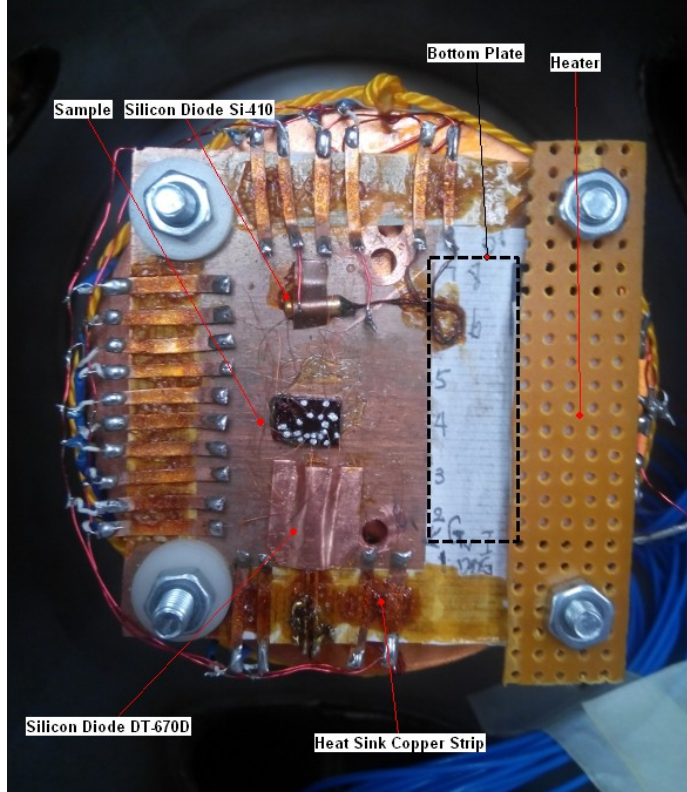
Figure 4.10: The sample platform on PT60.

where q is the heat flux and k is the thermal conductivity coefficient. For OFHC copper, $k \simeq 300 W \cdot m^{-1} \cdot K^{-1}$ at 100K. T_1 and T_0 are the temperatures at two ends. Here $T_0 = 100K$. The 35K bottom temperature of this setup shows about 10W heat transferred from the environment to the stage. Therefore the minimum cooling power at 100K is 60W. Since the cooling power of PT60 is 60W at 80K, T_1 will be 80K here. The thickness of two plates is $d = 6$mm. With these parameters, q is calculated to be $1MW/m^2$ and then the area of the bottom plate will be about $0.5 cm^2$. The actual size of the bottom block we used is about $3 cm^2$. Two facts result in a larger block. First, the stack is not a single piece but has two contact surfaces that reduce the heat conductivity even though Apiezon N cryogenic grease is applied between the surfaces. Secondly, the sample is not very close to the heater (the temperature has strong gradients near the heater). T_1 should be less than 100K. Two thermometers, Si-410 and DT-670D silicon diodes, are arranged at the two ends
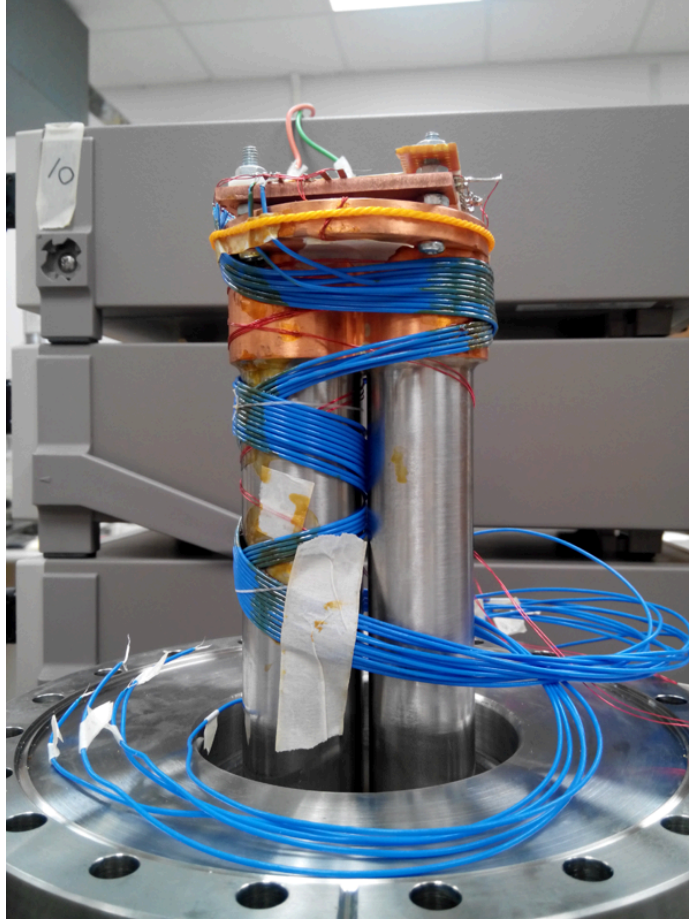
Figure 4.11: The wires on the cold stage of PT60 (Before the chamber is mounted.)

of the sample position. The temperature of the sample is the average of these two diodes.

In order to measure eight bridges at the same time, 16 LakeShore Type C Ultra Miniature coaxial cables plus 6 copper wires for two thermometers and one array of heaters are wired on the cryo stage (Fig. 4.11). Two coaxial cables are used on one bridge for the four-probe measurement. All voltage and current negative leads (metallic shields) of the coaxial cables are connected together to share the negative voltage and current electrodes on the sample pattern respectively as in Fig 4.12. The connections are through the $1cm \times 2mm$ copper strips that are glued on the plate by GE varnish (isolated by papers) to reduce the heat transferring into the sample. All the cables are glued by GE varnish and wrapped around the returning pulse tube to
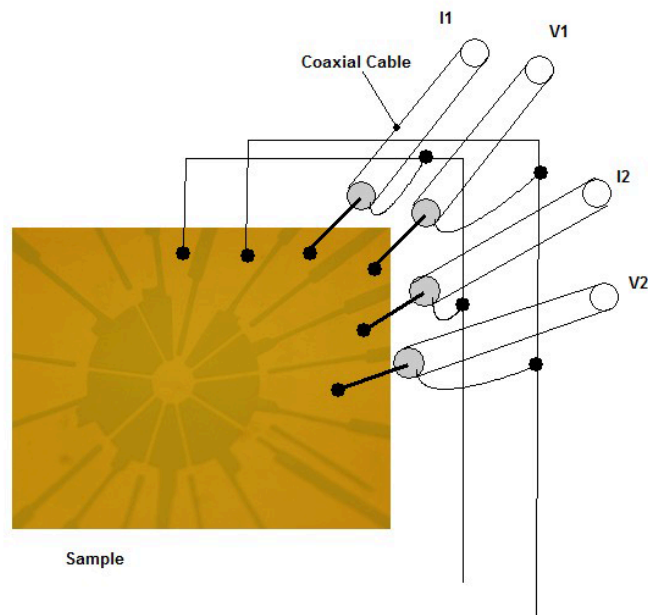
Figure 4.12: Electrical connections to the sample with the coaxial cables in PT60(only two pairs of cables are shown).

be cooled down by the returning gas.

The vacuum chamber is a tube of 304 stainless steel with 6 inch diameter. A 8 inch CF flange was mounted at one end of the tube(Fig. 4.13). Its another end is open but can be enclosed by a removable cap. It also has a DN25KF high vacuum flange to connect the vacuum station and two DN50KF flanges for two wire connectors. The wire connector is a flange cap with metal pins going through a high strength plastic plate (Fig. 4.14). Torr seal is used to glue the pins and the plastic plate on the aluminum cap.

4.3 Sound trigger system

With closed-cycle cryocoolers like the ones used in this work, the fact that the temperature oscillates with the cycle of the compressor is an inherent problem. A simple but novel approach was used to annul this temperature fluctuation in the following way: a microphone picks up the high pitched sound from the CP950 compressor as

44
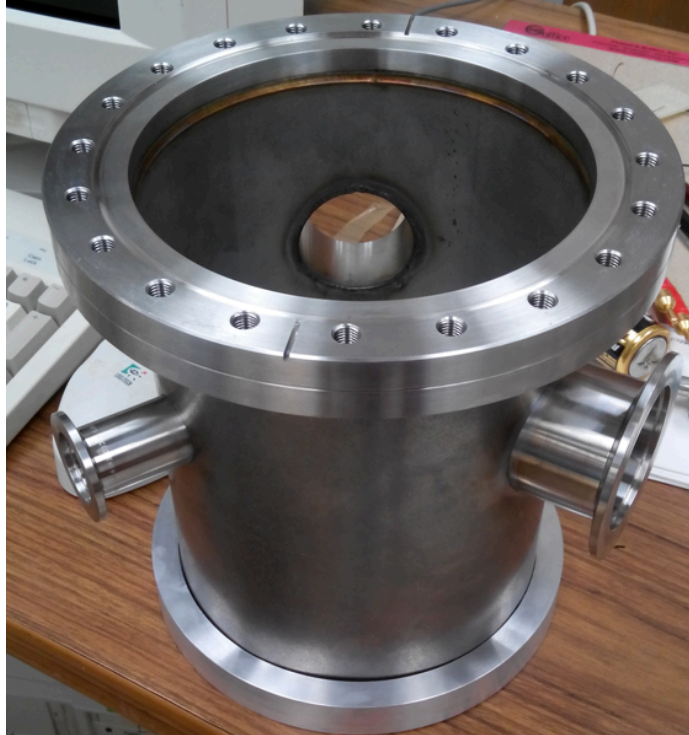
Figure 4.13: The vacuum chamber of PT60.

Figure 4.14: Wire connector on PT60(front and back).

in Fig. 4.15. The microphone output is fed to a pulse generator, Quantum Composer pulse generator Model 9512. Since the sound follows the frequency of the helium compression, the output signal from the pulse generator will be synchronized with the fluctuation of the temperature and this signal is fed to all measuring instruments. This reduces temperature errors from 0.2K to 0.05K.
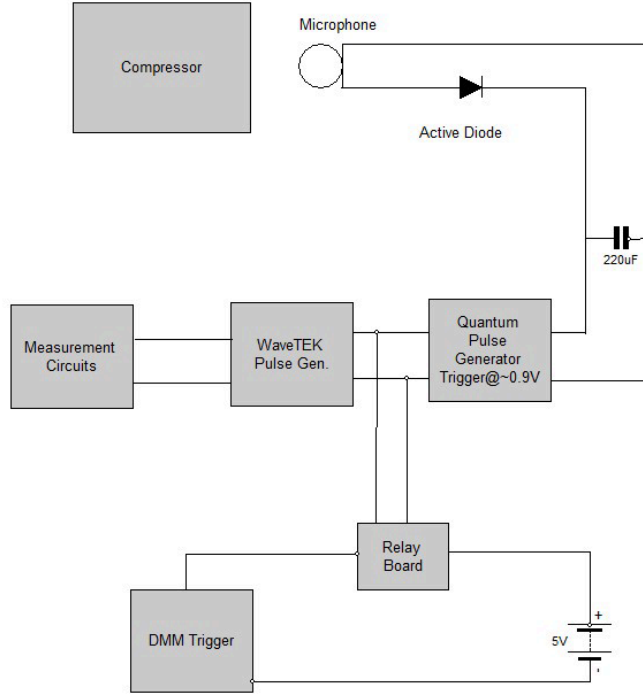
Figure 4.15: Diagram of the sound trigger system.

An active-diode circuit is used to cut off the negative part of the signal from the microphone. The positive part is integrated and smoothened by the capacitor. The Quantum Composer Pulse Generator has an adjustable triggering gate which can optimize the synchronization. In order to isolate the grounds between the pulse generator and the digital multimeters (DMMs), a relay is used for DMMs.

4.4 DC MEASUREMENT SETUP

A battery in series with a large resistance ($\sim$1 MΩ) served as a current source to apply a continuous $\sim 10\mu$A current to the sample (Fig. 4.16). A DPDT relay was used to switch the current direction to exclude the thermal emf and the contact resistance. Measuring the forward($+$) and reversed($-$) voltages of the sample and the standard resistor, the resistance of the sample could be calculated by

$$R = R_{std}\frac{\overline{V}^{+}_{sample} - \overline{V}^{-}_{sample}}{\overline{V}^{+}_{std} - \overline{V}^{-}_{std}}, \tag{4.2}$$
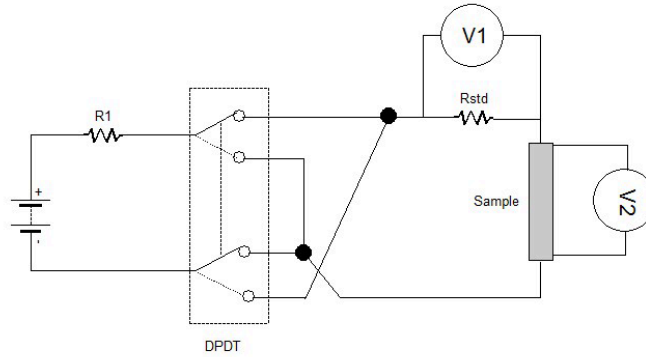
Figure 4.16: Circuit of DC 4-probe measurement. The Double Pole Double Throw (DPDT) relay is operated by the DAC card in the computer.

where all the voltages are the averages of the readings from DMMs.

4.5 PULSED MEASUREMENT SETUP

In a superconductor, high current densities will not only introduce the current-induced depairing but also cause the self heating effect and heat generation from the contacts. This is a major technical problem that is not easily overcome. In fact this is the reason that very few groups in the world are capable of measuring the depairing current and this important quantity has not been measured in the vast majority of superconductors. Information about this fundamental quantity, and information about the penetration depth that can be extracted from it, is crucial to the progress of this field. Our group's laboratory has leading expertise in overcoming these problems by using short-duration pulsed signals in place of continuous DC signals. Another advantage of the pulsed approach is thermal emf will be subtracted by the oscilloscope and hence it is not necessary to switch the direction of the current any more.

As shown in Fig. 4.17 the pulse generator, a Wavetek Model 801, provided a single-shot, constant amplitude pulse and synchronized the oscilloscope. The pulse was regulated by the current control device discussed in Sec. 4.6 and then feeded the current source which was composed by a fast-response transistor NTE 373 and a
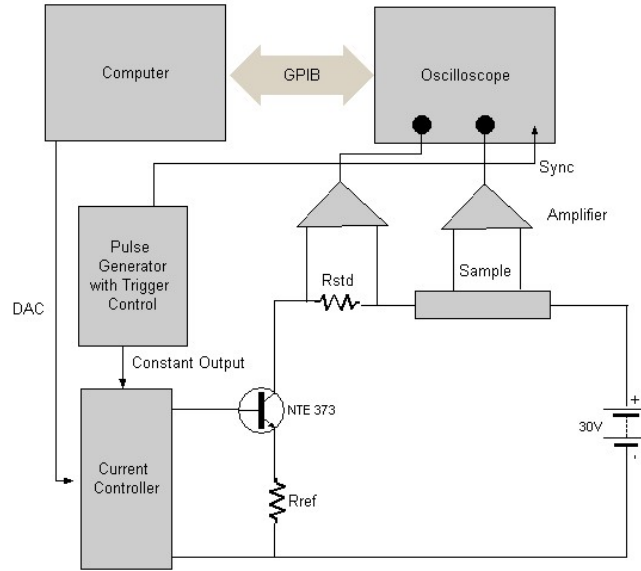
Figure 4.17: Puled measurement setup.

reference resistor. The current that went through the sample can be calculated by

$$I = \frac{V_{in} - V_{BE}}{R_{ref}} = \frac{V_{std}}{R_{std}},$$ (4.3)

where V_{in} is the voltage of the base and V_{BE} is the base-emitter bias of the transistor. The voltages were measured through the differential amplifier by the Lecroy 9341A oscilloscope. The computer can monitor the oscilloscope, collect data and adjust the current.

4.6   Electrically Isolated Devices for Controlling Current

The objective of these devices was to isolate the measuring circuit from the computer while automatically controlling the current. There were two different current control devices used in the experiments.

Stepper-motor-current controller

A stepper motor was used to rotate a linear-wire potentiometer (Fig. 4.18). It can provide an almost continuously changing current since the step of the motor is very
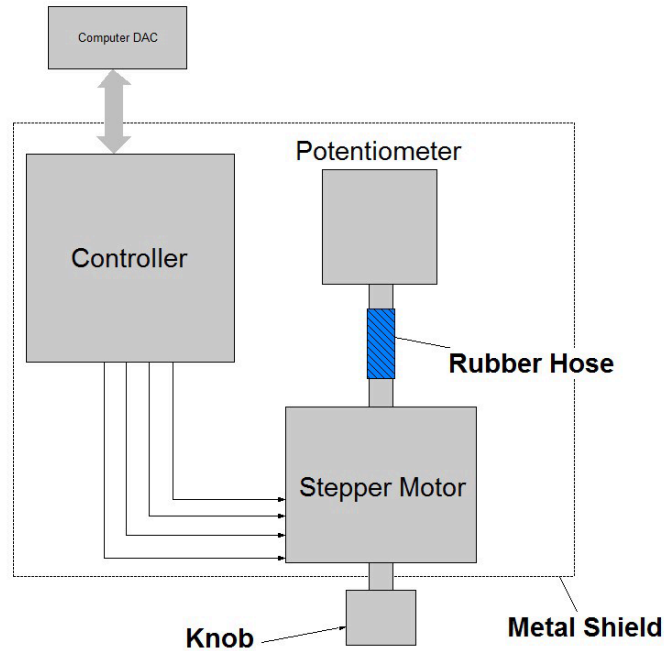
Figure 4.18: Diagram of the Motor-current-control.
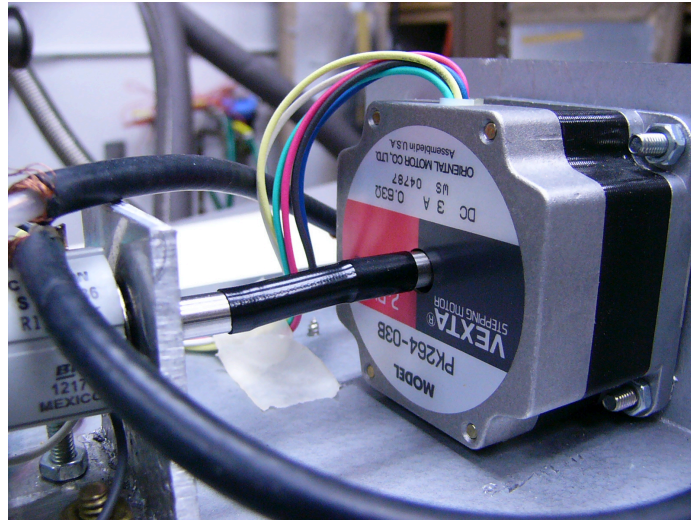
Figure 4.19: The rubber hose that connects the stepper motor and the potentiometer.

fine (about 1.8° per step) and the potentiometer has ten turns. Its disadvantage is that it is difficult to repeat a given current value.

The motor and the potentiometer were mounted coaxially and connected by a rubber hose which provided enough friction force to rotate the potentiometer without breaking it, even when turned beyond its limit (Fig. 4.19). The stepper motor model
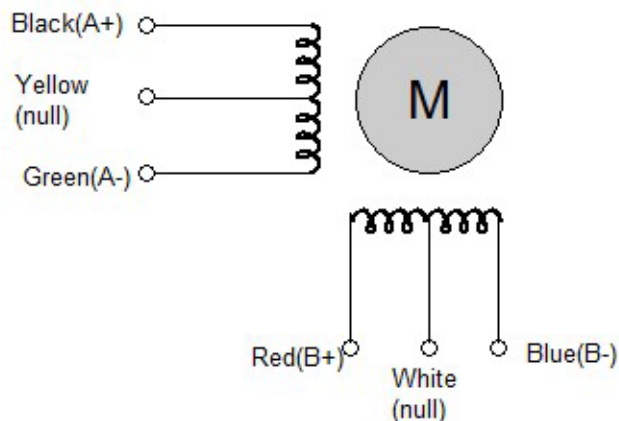
Figure 4.20: Diagram of the connections. A+, A-, B+ and B- represent the connectors on the controller (Fig. 4.21). The mark "null" means the wire is not connected.

is VEXTA PK264-03B. It's a 2-phase 6-lead wire type. The connections between the controller and the motor are present in Fig. 4.20. The controller requires both common wires of the motor to not be connected.

The controller of the stepper motor is Model M335-B-V1 (Fig. 4.21) which uses optocouplers to isolate the control circuit from the motor driving circuit (Fig. 4.22). Before connecting the computer to the controller, a power source which shares the same ground with the computer is required to be connected to "Source V+". This power supply is used to drive the LEDs in the optocouplers. An appropriate resistor is also necessary to be in series with LEDs depending on the voltage used. As stated in Fig. 4.22: for 5V, no resistor is required; for 12V, 1KΩ is required; for 24V, 2.7KΩ is required. Here, we used 5V which is compatible with the computer standard. To trigger one step, the voltage at "Pul-" must drop from 5V to 0; this is effected by the negative edge of a 1/10-second pulse generated by the digital lines of a computer DAC card under program control (Appendix C). The direction of the motor's rotation is governed by the voltage level (0 or 5V) of "Dir-". It is also necessary to set "EN-" (enable) to high (5V) to run the motor (if "EN-" is set to 0V, the motor will be disabled).
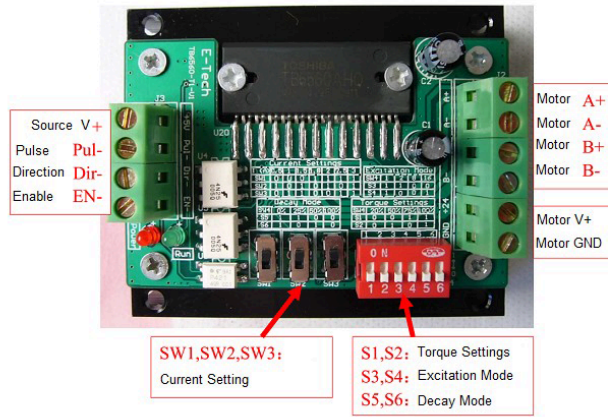
Figure 4.21: M335-B-V1 controller. (Translated from the Chinese manual)
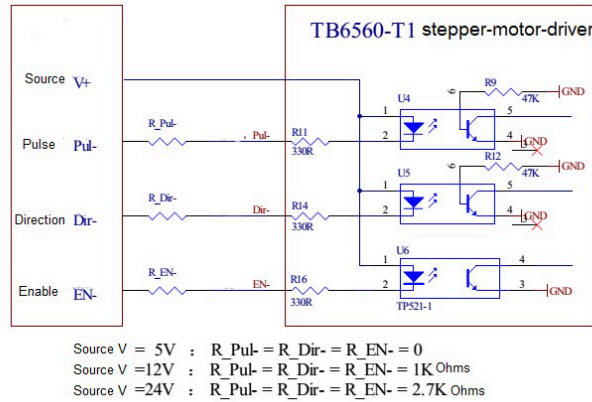
Figure 4.22: Diagram of M335-B-V1 controller. (Translated from the Chinese manual)

A "5V 3A" power supply provides power for the operation of the motor. This external power supply is connected across the "Motor V+" and "Motor GND" connectors. The running current of the motor is configured by three switches: SW1, SW2 and SW3. Table 4.1 shows the values of the current defined by the states of those switches. Since the motor needs 3A, we put all of these switches at position 1.

S1~S6 switches control the motion of the motor. S1 and S2 set the value of the torque when there is no step pulse sent in. That torque locks the motor until a larger torque is applied on the motor axial. We set S1 and S2 at position 0 because we

did not need a large torque. The excitation mode is defined by S3 and S4 as shown in Table 4.2 from the datasheet of the main chip TB6560AHQ. Here we found the 2W1-2-phase mode is best for our motor. S5 and S6 are used to smoothen the motion of the motor. We set them both to be 0.

Table 4.1: Current settings of M335-B-V1 controller

I(A)	0.5	1	1.5	1.8	2	2.5	3
SW1	0	0	0	1	1	1	1
SW2	1	0	1	0	1	0	1
SW3	0	1	1	0	0	1	1

Table 4.2: Excitation mode settings of M335-B-V1 controller

S3	S4	Excitation Mode
0	0	2-phase
0	1	1-2-phase
1	0	4W1-2-phase
1	1	2W1-2-phase

Relay-diode controller

A relay is usually a good option for the electrical isolation. As present in Fig. 4.23, each switch was controlled by a relay and only one would be closed at a time. Since the diode ECG597 has fixed forward bias ($\sim 0.56V$), the more diodes that are in series, the higher their combined voltage the. This voltage appears across the output terminal, which in turn controls the sample current. Thus the same current values are highly repeatable.
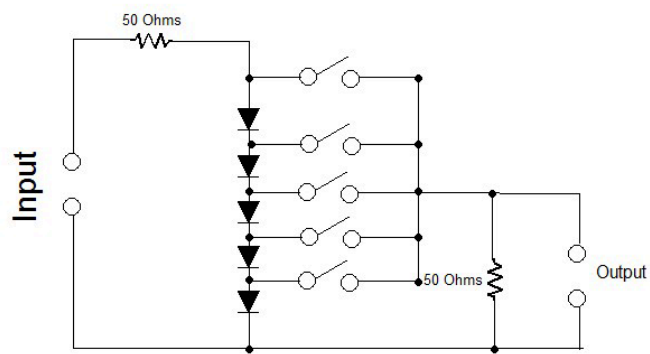
Figure 4.23: Circuit of the Diode-current-control.

Chapter 5

Data and Analysis

In this chapter, we will discuss the results of the measurements of two different samples: $Sr_{0.88}La_{0.12}CuO_2$ and $Nd_{1.85}Ce_{0.15}CuO_4$.

5.1 $Sr_{0.88}La_{0.12}CuO_2$

This sample was provided by our collaborators Li and coworkers in France. Single phase c-axis-oriented epitaxial thin films of $Sr_{0.88}La_{0.12}CuO_2$ (SLCO) were deposited on a heated $KTaO_3$ substrate by rf magnetron sputtering technique. As also emphasized in Ref. [29, 36], the choice of the substrate is essential for obtaining superconducting samples, as well as is an oxygen reduction step since the as-prepared films are insulating. The films were characterized by x-ray diffraction spectra which show that the films are epitaxial, highly c-axis-oriented (with a mosaicity of 0.1^o), and single phase with undetectable ($< 0.1\%$) impurity phases. The composition of SLCO deposits was checked by inductive-coupled plasma spectroscopy, giving x=0.12. The highest T_c obtained in this way for now is 26 K, the sample still being underdoped. The four-probe bridge measured in this work was patterned using photolithography followed by argon-ion milling. The bridge has the dimensions Fig. 5.1: thickness $t = 61$ nm, width $w = 6.2$ μm, and length $l = 97$ μm. Further details about sample preparation are provided elsewhere [37, 27].

The Cryomech PT405 cryostat was used. All depairing measurements were made in zero applied magnetic field. As shown in Ref. [31, 33, 30], micron-wide bridges typically have thermal resistances of order $R_{th} \sim 1$–10 nK.cm^3/W at microsecond
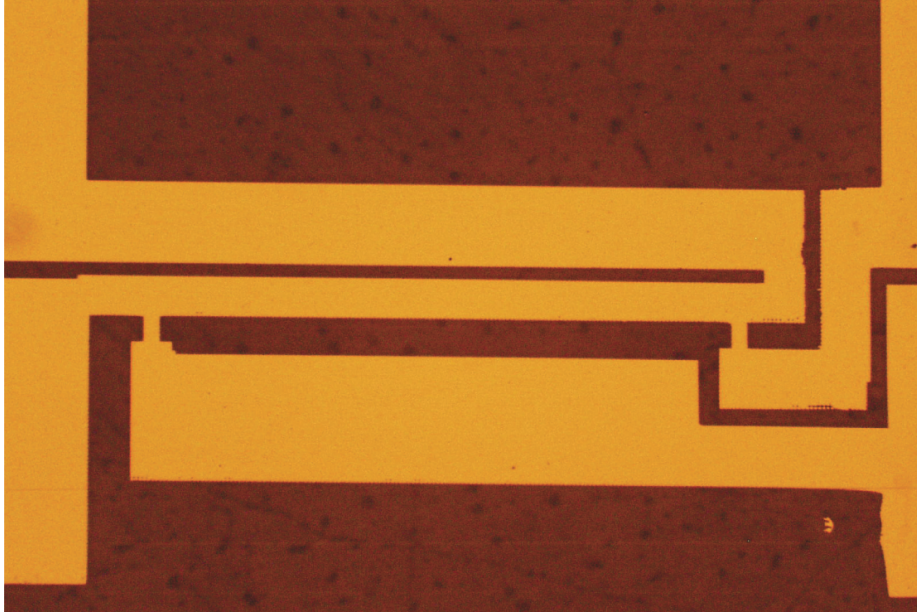
Figure 5.1: Pattern used for 4-probe measurement

timescales. The heat generated at contacts does not interfere with the bridge since the thermal diffusion distance ($\sqrt{Dt} \sim 10\mu$m) is much shorter than the contact-to-bridge distance (> 1 mm).

The pulse durations were around 5 μs with a pulse repetition period of about 1 s. 100 pulses were averaged to reduce the noise effect. As shown in Fig. 5.2, the pulse has a good shape plateau. This one was the voltage of the sample and measured with the amplifier at gain $= 10$. The two red upsidedown arrows indicate the portion used for the average of the signal. Another two green dashed arrows show the part for the average of the ground. The signal strength is obtained by the first average subtracting the second one and then dividing the gain.

Fig. 5.3(a) shows the resistive transitions in $B = 0$ at various applied currents. The lowest current of I=13 μA is of the continuous DC type; the rest are pulsed. The curves shift in a fairly parallel manner especially over the central portion in the vicinity of $R \sim R_n/2$, as emphasized in the inset. We define the depairing current $I_d(T)$ at a given temperature T at the midpoint of the resistive transition $R = R_n/2 = 98\Omega$. (As shown elsewhere[34], variations in film thickness can cause

55
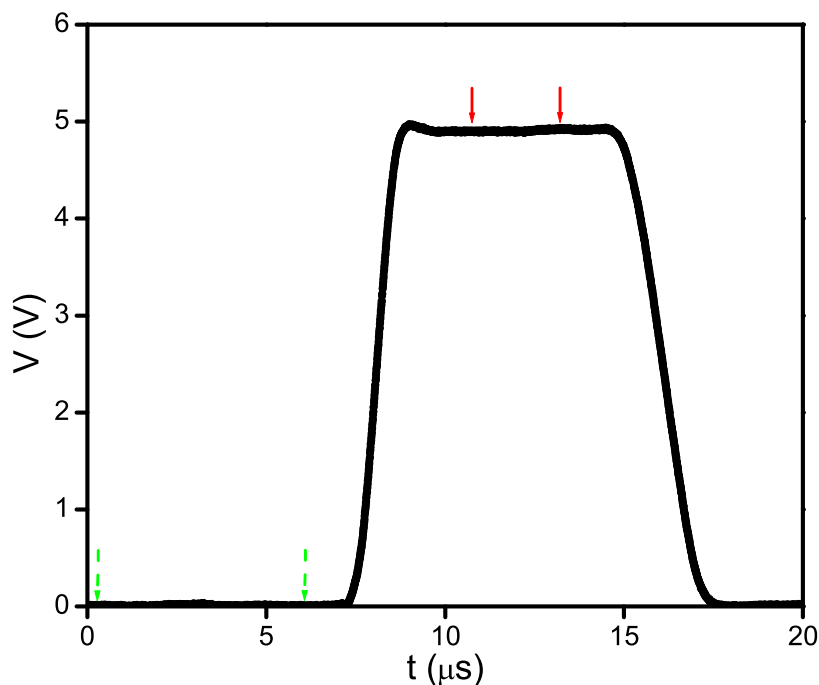
Figure 5.2: Pulse used for $Sr_{0.88}La_{0.12}CuO_2$ 4-probe measurement.

transitions to broaden with increasing j with a functional shape given by $R(j,T,\delta t) = R_n\{\log(j/4j_d(0)) - 1.5\log(1 - T/T_c)\}/\log(1 + \delta t/t)$, where δt=thickness variation. At the $R_n/2$ criterion (shown by the dashed line) the actual T_c shifts correspond exactly to shifts for a sample with the same mean thickness t but with $\delta t = 0$.) Panel (b) of Fig. 5.3 shows plots against T, of $I_d^{2/3}$ (corresponding to the pair breaking effect) and I_d^2 (corresponding to Joule heating). The two-thirds power is clearly seen to hold, confirming current induced depairing. From the y-axis intercept of the $I_d^{2/3}(T)$ versus T curve we find the zero-temperature value [32] to be $I_d(0) \approx 0.25[T_c dI^{2/3}/dT]^{3/2} = 21$ mA. The corresponding value of the zero-temperature depairing current density is $j_d(0) = 5.9$ MA/cm^2. (In a full nodal d-wave superconductor, one can expect an anisotropy in j_d as a function of the in-plane angle resulting in a $\sqrt{2}$ modulation at $T = 0$. However this anisotropy is washed out in the high temperature region of interest here. Furthermore, as shown in Chap. 3, interactions between electrons and

antiferromagnetism in this system, results in the nodes being pushed below the Fermi level.)
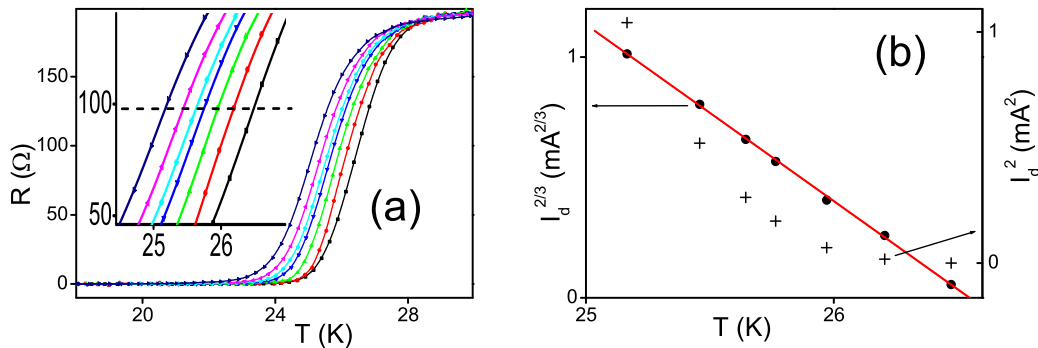
Figure 5.3: (a) Resistive transitions for $Sr_{0.88}La_{0.12}CuO_2$ in zero magnetic field at transport current values of (right to left): 12.9, 132, 258, 426, 533, 721, and 1020 μA. The lowest current is continuous DC; the remaining currents are pulsed. (b) Two-thirds power of the depairing current versus the midpoint transition temperature.

$j_d(0)$ can be related to the upper critical field B_{c2} and the magnetic penetration depth λ. Since the $B_{c2}(T, j)$ boundary is itself a function of j, we obtain B_{c2} for this sample by measuring the shift in the resistive transition by a magnetic field at the same high applied current value of I = 1.02 mA (which corresponds to the left most curve of Fig. 5.3(a)). Fig. 5.4(a) shows these resistive transitions in various perpendicular magnetic fields B. As discussed elsewhere [32, 51, 17] increased dissipation at higher values of B and I promote a more uniform current-flow profile and provide a truer sampling of the bulk properties.

In a very weak pinning system (such as amorphous molybdenum-germanium), some progressive broadening with increasing B can be expected because of flux motion [39]. However the cuprates have stronger pinning and consequently the R–T curves are fairly parallel here. Defining B_{c2} at the midpoint of the transition yields the $B_{c2}(T)$ curve shown in Fig. 5.4(b), with a corresponding value of $B_{c2}(0) \approx 0.7 \, T_c \, dB_{c2}(T)/dT = 5.1$ T for this sample at the 1 mA current, as per

the WHH formalism [61, 25]. The penetration depth for this system was measured by Fruchter *et al.* [15] for various doping levels and transition temperatures. From their Table I, extrapolating to our T_c, we expect $\lambda(T = 0) \approx 0.5~\mu$m. Using Eq. 2.12, $j_d(0) = 5.56 \times 10^{-3}\sqrt{B_{c2}}/\lambda^2$ gives a theoretical value of $j_d(0) = 5$ MA/cm^2, in agreement with our measured value 5.9 MA/cm^2.
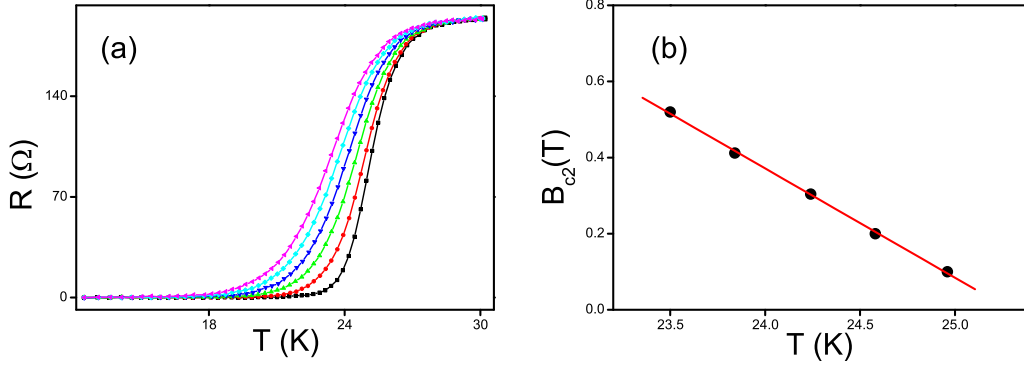
Figure 5.4: (a) Resistive transitions for $Sr_{0.88}La_{0.12}CuO_2$ at a current of I $= 1.02$ mA in perpendicular magnetic field values of (right to left): 0, 0.1, 0.2, 0.304, 0.412, 0.52 T. (b) Upper critical magnetic field versus the midpoint transition temperature.

5.2 $Nd_{1.85}Ce_{0.15}CuO_4$

This sample was provided by Guarino and coworkers in Italy. The $Nd_{1.85}Ce_{0.15}CuO_4$ (NCCO) films were grown on (001)-oriented SrTiO$_3$ (STO) substrates by dc sputtering technique in on-axis configuration. A single stoichiometric target of NCCO, prepared by standard solid-state reaction, was used as a sputtering source. The samples were deposited at 850 ^{o}C in a mixed atmosphere of Ar and O$_2$, in the ratio O$_2$/Ar $\sim$1, at a power equal to 12 W. The films were annealed in vacuum for about 30 minutes at the same growth temperature. Additional heat treatment needed to induce superconductivity via further reduction of the oxygen content was performed

ex-situ in an ambient atmosphere of Ar above 850 ^{o}C. The film was grown at the rate of 1.2 nm/min.

Film quality was monitored by X-ray diffraction measurements by means of a Philips X'Pert-MRD PRO high resolution diffractometer equipped with a four circle cradle. Composition analysis was performed by using a scanning electron microscope LEO EVO50 equipped with an Oxford Wave 700 wavelength dispersive spectrometer. The detector, which collects the x-ray spectrum starting from elements with $Z \geq 4$, allows for a precise assessment of the Ce content, x, in the structure. Fig. 5.5 shows a typical $\theta - 2\theta$ x-ray diffractogram of the (00l) NCCO Bragg reflections. It shows a well oriented film with the c-axis of NCCO structure normal to the surface of the sample. The inset of Fig. 5.5 shows the rocking curve around the (004) reflection of the NCCO phase. The full width at half maximum (FWHM) is equal to 0.3 deg.

The four-probe bridge measured in this work was patterned using photolithography followed by wet etching in a 1% aqueous solution of H_3PO_4. The bridge in Fig. 5.6 has the dimensions: thickness $t = 250$ nm, width $w = 50$ μm, and length $l = 1.92$ mm. T_c we found is ~ 21K. Further details about sample preparation are provided elsewhere [20, 9, 59].

Fig. 5.7(a) shows resistive transitions in $B = 0$ at various applied currents. As per the justification given in SLCO, we define the depairing current $I_d(T)$ at a given temperature T at the midpoint of the resistive transition $R = R_n/2 = 7.25\Omega$. Panel (b) of Fig. 5.7 shows plots against T of $I_d^{2/3}$ (corresponding to the pair breaking effect) and I_d^2 (corresponding to Joule heating). The two-thirds power is clearly seen to hold, confirming current induced depairing. From the y-axis intercept of the $I_d^{2/3}(T)$ versus T curve we find the zero-temperature value to be $I_d(0) \approx 0.25[T_c dI^{2/3}/dT]^{3/2} = 453$ mA. The corresponding value of the zero-temperature depairing current density is $j_d(0) = 3.63$ MA/cm^2.

Again, B_{c2} can be obtained from the transport measurements, by measuring re-
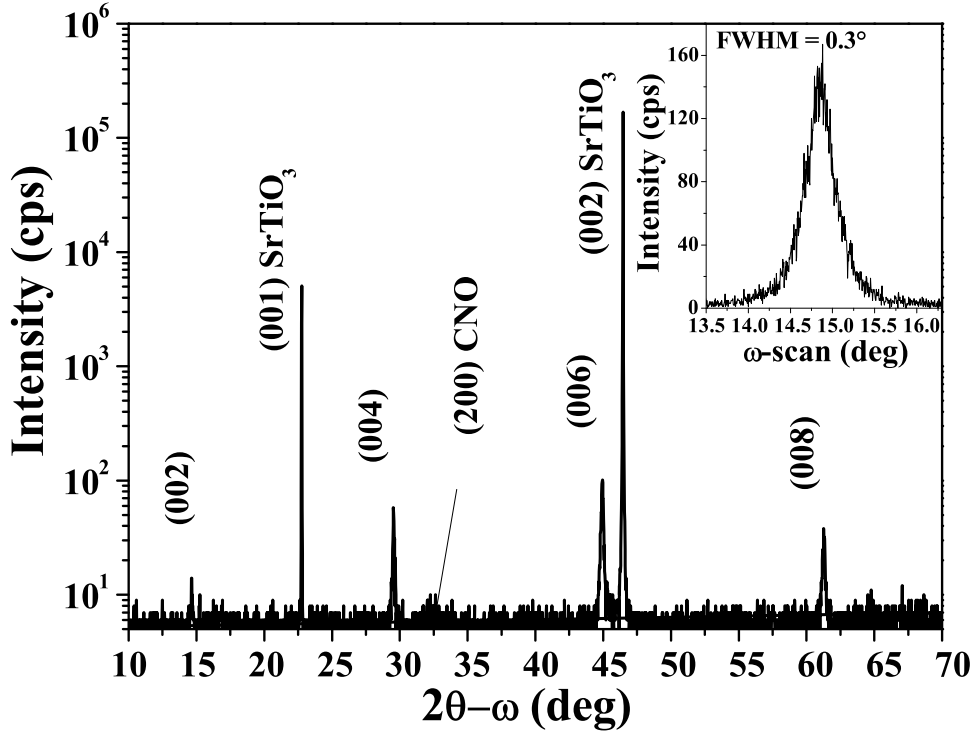
Figure 5.5: X-ray diffractogram of the $Nd_{1.85}Ce_{0.15}CuO_4$ film sample. The inset shows the rocking curve around the (004) reflection with a FWHM of about 0.3 deg.
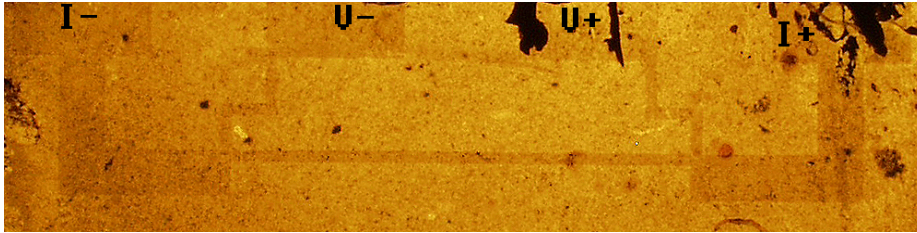
Figure 5.6: The $Nd_{1.85}Ce_{0.15}CuO_4$ sample. The photo was taken with backlight. Therefore, the grains from the back side are obvious in the graph.

sistive transitions in various perpendicular magnetic fields B, which are shown in Fig. 5.8(a). To make the two resistive-transition measurements ($R(T)$ at various j and $R(T)$ at various B) compatible for comparison, we use a similar high pulsed current of $I = 34$ mA as that in SLCO. As a result high currents provide for a truer sampling of the bulk properties and a more meaningful comparison between the two sets of resistive transitions, even though the pair breaking action of using a high j
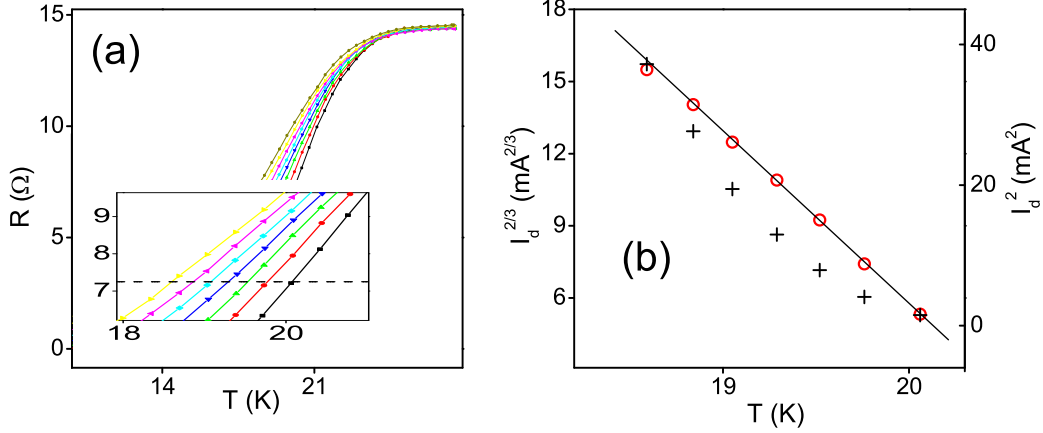
Figure 5.7: (a) Resistive transitions in zero magnetic field at transport current values of (right to left): 12.3, 20.2, 28.1, 36, 44.1, 52.6, 61 mA. The inset shows the central portion, with the horizontal dashed line indicating the $R_n/2$ level. (b) Two-thirds power (left axis, circles) and square power (right axis, plus symbols) of the applied current versus the midpoint transition temperature, corresponding to current induced depairing and Joule heating respectively.

($\sim 7.5\%$ of $j_d(0)$) will slightly reduce the obtained estimate of B_{c2}. Defining B_{c2} at the midpoint of the transition yields the $B_{c2}(T)$ curve shown in Fig. 5.8(b), with a corresponding value of $B_{c2}(0) \approx 0.7 \ T_c \ dB_{c2}(T)/dT = 2.14$ T for this sample at the 34 mA current. Because of the absence literature on the value of λ in NCCO, we use the relation $j_d(0) = 5.56 \times 10^{-3} \sqrt{B_{c2}(0)}/\lambda(0)^2$ to compute it, as $\lambda(0) = 0.47 \ \mu$m. In the literature, we did not find a direct absolute measurement of $\lambda(0)$ because of the aforementioned difficulties associated with the Nd^{3+} paramagnetic moments; however, we expect the value of this quantity to be comparable to that in the sister electron-doped compound $Pr_{2-x}Ce_xCuO_{4-\delta}$ (PCCO) but somewhat longer because of the greater pair breaking in NCCO compared to PCCO. In PCCO we find [49] $\lambda(0) = 0.25 \ \mu$m, which is indeed of the same order as our $\lambda(0)$ found for NCCO and somewhat shorter.
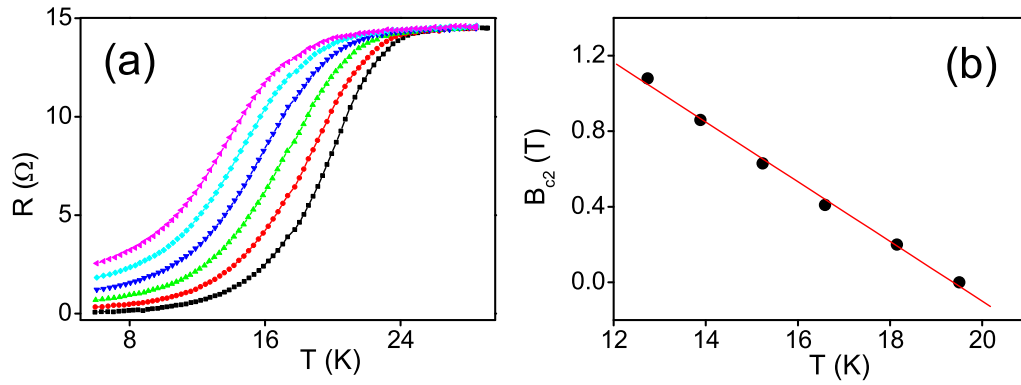
Figure 5.8: (a) Resistive transitions at a current of I = 34 mA ($j = 272$ kA/cm^2) in perpendicular magnetic field values of (right to left): 0, 0.2, 0.41, 0.63, 0.86, and 1.08 T. (b) Upper critical magnetic field versus the midpoint transition temperature.

Conclusion

We have studied current-induced pair-breaking in two different cuprate electron-doped superconductors, $Sr_{0.88}La_{0.12}CuO_{2+x}$ and $Nd_{1.85}Ce_{0.15}CuO_4$, near T_c and found the measured $j_d(T)$ function to conform exactly with the $\Delta T_c \propto j^{2/3}$ Ginzburg-Landau form. The extracted value of $j_d(0)$ of SLCO is in good agreement with the value obtained from the B_{c2} and λ parameters, which brings up a useful point: these combined self-consistent measurements of $B_{c2}(T)$ and $j_d(T)$ provide a useful method for obtaining λ purely from transport measurement in a bridge, which was adopted in the analysis of NCCO. This should be of special value in situations where the volume, area, or geometry make the sample unsuitable for penetration depth measurements using inductive methods. The low value of j_d is consistent with the large penetration depths and implied low superfluid densities in this system, related to a low carrier concentration and/or strong disorder [15].

BIBLIOGRAPHY

[1] N. P. Armitage, P. Fournier, and R. L. Greene, Rev. Mod. Phys. **82** (2010), 2421.

[2] R. Arpaia, S. Nawaz, F. Lombardi, and T. Bauch, IEEE Trans Appl. Super. **23** (2013), 1101505.

[3] J. Bardeen, Rev. Mod. Phys. **34** (1962), 667.

[4] J. Bardeen, L. N. Cooper, and J. R. Schrieffer, Phys. Rev. **108** (1957), 1175.

[5] J. G. Bednorz and K. A. Müller, Z. Phys. **B64** (1986), 189.

[6] N. N. Bogoliubov, Nuovo Cimento **7** (1958), 794, *Zh. Eksperim. i. Teor. Fiz.* **34**, 58 (1958)[*Soviet Phys.*-JETP **7** (1958), 41].

[7] Jr. Charles P. Poole, Horacio A. Farach, and Richard J. Creswick, *Superconductivity*, Academic Press, Inc., 1995.

[8] C.-T. Chen, P. Seneor, N.-C. Yeh, R. P. Vasquez, L. D. Bell, C. U. Jung, J. Y. Kim, M. Park, H. Kim, and S. Lee, Phys. Rev. Lett. **88** (2002), 227002.

[9] C. Cirillo, A. Guarino, A. Nigro, and C. Attanasio, Phys. Rev. B **79** (2009), 144524.

[10] C. Cirillo, A. Rusanov, C. Bell, and J. Aarts, Phys. Rev. B **75** (2007), 174510.

[11] L. N. Cooper, Phys. Rev. **104** (1956), 1189.

[12] E. Dagotto, Rev. Mod. Phys. **66** (1994), 763.

[13] D. Dew-Hughes, Low Temp. Phys. **27** (2001), 713.

[14] H. Fröhlich, Phys. Rev. **79** (1950), 845.

[15] L. Fruchter, V. Jovanovic, H. Raffy, Sid Labdi, F. Bouquet, and Z. Z. Li, Phys. Rev. B **82** (2010), 144529.

[16] J. R. Gavaler, Appl. Phys. Lett. **23** (1973), 480.

[17] J. M. E. Geers, M. B. S. Hesselberth, J. Aarts, and A.A. Golobuv, Phys. Rev. B **64** (2001), 94506.

[18] V. L. Ginzburg and L. D. Landau, Zh. Eksperim. i. Teor. Fiz. **20** (1950), 1064.

[19] L. P. Gor'kov, Zh. Eksperim. i. Teor. Fiz. **36** (1959), 1918, [*Soviet Phys.*-JETP **9**(1959), 1364].

[20] A. Guarino, R. Fittipaldi, A. Romano, A. Vecchione, and A. Nigro, Thin Solid Films **524** (2012), 282.

[21] A. Gurevich, Rep. Prog. Phys. **74** (2011), 124501.

[22] D. J. Van Harlingen, Rev. Mod. Phys. **67** (1995), 515.

[23] D. R. Harshman and Jr. A. P. Mills, Phys. Rev. Lett. **67** (1992), 10684.

[24] J. W. Harter, L. Maritato, D. E. Shai, E. J. Monkman, Y. Nie, D. G. Schlom, and K. M. Shen, Phys. Rev. Lett. **109** (2012), 267001.

[25] E. Helfand and N. R. Werthamer, Phys. Rev. **147** (1966), 288.

[26] S. Hikami, T. Hirai, and S. Kagoshima, Jpn. J. Appl. Phys. **26** (1987), L314.

[27] V. Jovanovic, Z. Z. Li, F. Bouquet, L. Fruchter, and H. Raffy, J. Phys. **150** (2009), 052086.

[28] Y. Kamihara, H. Hiramatsu, M. Hirano, R. Kawamura, H. Yanagi, T. Kamiya, and H. Hosono, J. Am. Chem. Soc. **128** (2006), 10012.

[29] S. I. Karimoto, K. Ueda, M. Naito, and T. Imai, Appl. Phys. Lett. **79** (2001), 2767.

[30] M. N. Kunchur, Mod. Phys. Lett. B **9** (1995), 399.

[31] ——, Phys. Rev. Lett. **89** (2002), 137005.

[32] ——, J. Phys.: Condens. Matter **16** (2004), R1183.

[33] M. N. Kunchur, B. I. Ivlev, D. K. Christen, and J. M. Phillips, Phys. Rev. Lett. **84** (2000), 5204.

[34] M. N. Kunchur, Sung-Ik Lee, and W. N. Kang, Phys. Rev. B **68** (2003), 064516.

[35] W. Langa, I. Puica, K. Siraj, M. Peruzzi, J. D. Pedarnig, and D. Bäuerle, Physica C **460** (2007), 827.

[36] V. Leca, D. H. A. Blank, G. Rijnders, S. Bals, and G. Van Tendeloo, Appl. Phys. Lett. **89** (2006), 092504.

[37] Z. Z. Li, V. Jovanovic, H. Raffy, and S. Megtert, Physica C **469** (2009), 73.

[38] M. Liang and M. N. Kunchur, Phys. Rev. B **82** (2010), 144517.

[39] M. Liang, M. N. Kunchur, J. Hua, and Z. Xiao, Phys. Rev. B **82** (2010), 064502.

[40] F. London and H. London, Proc. Roy. Soc.(London) **A149** (1935), 71.

[41] M. Yu. Kupriyanovand V. F. Lukichev, Fiz. Nizk. Temp. **6** (1980), 445, [*Sov. J. Low Temp. Phys.*-JETP **6**(1980), 210].

[42] K. Maki, Prog. Theor. Phys. **29** (1963), 333.

[43] P. K. Mang, S. Larochelle2, A. Mehta, O. P. Vajk, A. S. Erickson, L. Lu, W. J. L. Buyers, A. F. Marshall, K. Prokes, and M. Greven, Phys. Rev. B **70** (2004), 094507.

[44] W. Meissner and R. Ochsenfeld, Naturwissenschaft **21** (1933), 787.

[45] E. J. Nicol and J. P. Carbotte, Phys. Rev. B **43** (1991), 10210.

[46] H. K. Onnes, Leiden Commun. (1911), 120b, 122b, 124c.

[47] Yu. N. Ovchinnikov, Zh. Eksp. Teor. Fiz. **56** (1969), 1590, [*Sov. Phys.*-JETP **29**(1969), 853].

[48] A. Podlesnyaka, A. Mirmelsteina, A. Voronina, B. Goshchitskiia, T. D'yachkovab, H. Kadyrovab, V. Zubkovb, Yu. Zainulinb, V. Kochetkovc, E. Khlybovc, R. Rosenkranzd, and A. FurrerCorresponding, Physica C **230** (1994), 311.

[49] R. Prozorov, R. W. Giannetta, A. Carrington, P. Fournier, R. L. Greene, P. Guptasarma, D. G. Hinks, and A. R. Banks, Appl. Phys. Lett. **77** (2000), 4202.

[50] J. Romijn, T. M. Klapwijk, M. J. Renne, and J. E. Mooij, Phys. Rev. B **26** (1982), 3648.

[51] A. Yu. Rusanov, M. B. S. Hesselberth, and J. Aarts, Phys. Rev. B **70** (2004), 024510.

[52] K. H. Satoh, S. Takeshita, A. Koda, R. Kadono, K. Ishida, S. Pyon, T. Sasagawa, and H. Takagi, Phys. Rev. B **77** (2008), 224503.

[53] D. J. Scalapino, Phys. Rep. **250** (1995), 329.

[54] M. Sigrist and T. M. Rice, J. Phys. Soc. Jpn. **61** (1992), 4283.

[55] G. R. Stewart, Rev. Mod. Phys. **83** (2011), 1589.

[56] H. Takagi, S. Uchida, and Y. Tokura, Phys. Rev. Lett. **62** (1989), 1197.

[57] Michael Tinkham, *Introdution to superconductivity*, McGraw Hill, 1996.

[58] Y. Tokura, H. Takagi, and S. Uchida, Nature **337** (1989), 345.

[59] S. Uthayakumar, R. Fittipaldi, A. Guarino, A. Vecchione, A. Romano, A. Nigro, H.-U. Habermeier, and S. Pace, Physica C **468** (2008), 2271.

[60] J. Wang, Z. Rak, F. Zhang anb R.C. Ewing, and U. Becker, J. Phys.: Condens. Matter **23** (2011), 465503.

[61] N. R. Werthamer, E. Helfand, and P. C. Hohenberg, Phys. Rev. **147** (1966), 295.

[62] D. A. Wollman, D. J. Van Harlingen, J. Giapintzakis, and D. M. Ginsberg, Phys. Rev. Lett. **74** (1995), 797.

[63] D. A. Wollman, D. J. Van Harlingen, W. C. Lee, D. M. Ginsberg, and A. J. Leggett, Phys. Rev. Lett. **71** (1993), 2134.

[64] H. Won and K. Maki, Phys. Rev. B **49** (1994), 1397.

[65] M. K. Wu, J. R. Ashburn, C. J. Torng, P. H. Hor, R. L. Meng, L. Gao, Z. J. Huang, Y. Q. Wang, , and C. W. Chu, Phys. Rev. Lett. **58** (1987), 908.

[66] Z. X. Zhao, L. Q. Chen, Q. S. Yang, Y. Z. Huang, G. H. Chen, R. M. Tang, G. R. Liu, G. C. Cui, L. Chen, L. Z. Wang, S. Q. Guo, S. L. Li, J. Z., and Bi, Kexue Tongbao **33** (1987), 661.

APPENDIX A

C CODE FOR Δ COMPUTATION

The energy gaps Δ of s-wave in Eq. 1.46 and d-wave in Eq. 1.53 can be calculated by the following programs. The shared function *fpts* is from "Commonly used algorithm of C procedures", 3rd Edition. Or it can be replaced by other integral routines. The file *elliptic.c*, which contains the functions for the complete elliptic integrals of the first and second kind, is from *http://www.netdenizen.com/emagnet/offaxis/elliptic_c.htm* by E. Dennison.

s-wave

```c
#include <stdio.h>

#include <stdlib.h>

#include "math.h"

#include "9FPTS.C"

//char filename[] = "BCS_NUMERICAL_RESULT_NV0_1.txt";

//const double NV = 0.1; //N(0)V

//const double w = 19426.09813; // \hbar \omega_c

char filename[] = "BCS_NV0_01_W_Infi.txt";

const double NV = 0.01; //N(0)V

const double w = 2.357997493E+043; // \hbar \omega_c

//const double w = 19426.09813;

const double GAP0 = 1.764; // \Delta(0)

const double esp = 1e-6;   //Precision

const double d = 1e-6;

/*
```

```c
with these constants, we have kTc = 1;

All energy quantities are in unit of kTc.
*/
double    GAP, T;  //\Delta(t) and Temperature;


double Integrant(double epsilon)
{
     double temp;
     temp = sqrt(pow(epsilon,2.)+pow(GAP,2.));
     return   (tanh(0.5/T*temp)/temp);
}
int main(int argc, char *argv[])
{
  FILE * file;
  file = fopen(filename, "w");
  fclose(file);
  GAP = GAP0;                                  // should be a little larger
     than \Delta(0)
  for(T = 0.01; T<=1.; T += 0.0001)
  {
      printf("T = %E, GAP = %E\n", T, GAP);
      for(;!(fabs(1/NV-fpts(0.,w,esp*100,d,Integrant)) < esp);)
      {
          GAP -= d;
          if(GAP < 0.) { T = 2.; break;}
      }
      file = fopen(filename, "a");
      fprintf(file, "%f, %.10f\n", T, GAP);
      fclose(file);
```

```c
  }

  return 0;

}
```

d-wave

```c
/* Follow the formula in PRB 46, 1397(1994) */

#include <stdio.h>

#include <stdlib.h>

#include "math.h"

#include "9FPTS.C"

#include "elliptic.c"

char filename[] = "DWave_NV0_1_W_Infi.txt";

const double w = 50; // \hbar \omega_c

const double PI = 3.14159265;

const double GAP0 = 2.13977795; // \Delta(0)

const double esp = 1e-6;   //Precision

const double d = 1e-8;

double    GAP, T, GoT;

double        kk2 = 0.5;

double Integrant(double x)

{

        double temp, fk, fe;

        int ierr;

        temp = 1/(1+exp(GoT*x));

        if(x > 1){

                fk = F(1/x, ierr);

                fe = FastE(fk, 1/x, ierr);

                temp = x*temp;

        }
```

```c
        else if(x < 1){

                fk = F(x, ierr);

                fe = FastE(fk, x, ierr);

        }

        else{

                return 0;

        }

        return  temp * (fk-fe);

}

double RHS(){

        double temp;

        GoT = GAP/T;

        temp = 8/PI*(fpts(0., 1-d, esp, d, Integrant) + fpts(1+d, w/GAP,

            esp, d, Integrant));

        return temp;

}

int main(int argc, char *argv[])

{

  FILE * file;

  double newGAP;

  file = fopen(filename, "w");

  fclose(file);

  GAP = GAP0 + 0.01;

  for(T = 0.01; T<=1.; T += 0.005)

  {

        printf("T = %E, GAP = %E\n", T, GAP);

        while(1)

        {

                newGAP = GAP0/exp(RHS());
```

```c
            if(fabs(GAP-newGAP) < esp) break;

            GAP = newGAP;

        }

        file = fopen(filename, "a");

        fprintf(file, "%f, %.10f\n", T, GAP);

        fclose(file);

    }

    return 0;

}
```

Appendix B

C code for the thermometers

Here are two functions used to convert the voltage readings from the diodes to temperatures. The binary search algorithm is used in both functions to search the standard temperature response tables. To use, just call the function DT670_CONVERT for DT670 diode and Si410_CONVERT for Si-410 diode with passing the measured voltages as the parameters. Both of them should use a $10\mu A$ current source as excitation. If the temperature is out of range, they will return -1 as an error.

Diode_DT670.h

```
#define DT670_NUM 66


double DT670_VArray[DT670_NUM] = {

        0.536542, 0.548102, 0.559639, 0.582637, 0.605528, 0.621141,

            0.628302, 0.650949, 0.673462,

        0.695834, 0.718054, 0.740115, 0.762007, 0.783720, 0.794505,

            0.805242, 0.815928, 0.826560,

        0.837138, 0.847659, 0.858120, 0.868518, 0.878851, 0.889114,

            0.899304, 0.909416, 0.919446,

        0.929390, 0.939242, 0.949000, 0.958657, 0.968209, 0.977650,

            0.986974, 0.996174, 1.005244,

        1.014181, 1.022984, 1.027594, 1.031651, 1.040183, 1.048584,

            1.056862, 1.060141, 1.063403,

        1.066650, 1.069881, 1.073099, 1.076303, 1.079492, 1.082669,

            1.085842, 1.089024, 1.090627,
```

```
        1.092244, 1.093878, 1.095534, 1.097216, 1.098930, 1.100681,

            1.102476, 1.104324, 1.016244,

        1.108261, 1.110421, 1.112810

};


double DT670_TArray[DT670_NUM] = {

        310, 305, 300, 290, 280, 273.15, 270, 260, 250, 240, 230,

        220, 210, 200, 195, 190, 185, 180, 175, 170, 165, 160, 155,

        150, 145, 140, 135, 130, 125, 120, 115, 110, 105, 100, 95,

        90, 85, 80, 77.35, 75, 70, 65, 60, 58, 56, 54, 52, 50, 48,

        46, 44, 42, 40, 39, 38, 37, 36, 35, 34, 33, 32, 31, 30, 29, 28, 27

};


double DT670_CONVERT(double v){

        int left = 0, right = DT670_NUM - 1;

        int mid = (left + right) / 2;

        if((v < DT670_VArray[0]) || (v > DT670_VArray[DT670_NUM - 1]))

                    return -1;

        while(left != right){

                if(v < DT670_VArray[mid])

                        right = mid;

                else

                        left = mid;

                mid = (left + right) / 2;

                if(left == mid || right == mid)

                        break;

        }

        if(DT670_VArray[mid] > v){

                left = mid;
```

```
                    right = mid - 1;

        }

        else{

                    left = mid + 1;

                    right = mid;

        }

        return (DT670_TArray[left] + (v -

            DT670_VArray[left])/(DT670_VArray[right] - DT670_VArray[left])

                *(DT670_TArray[right] - DT670_TArray[left]));

}
```

Diode_SI410.h

```
#define DSi410_NUM 309


double Si410_Array[DSi410_NUM] = {

        1.7191, 1.7086, 1.6852, 1.6530, 1.6124, 1.5659, 1.5179, 1.4723,

                1.4309,

        1.3956, 1.3656, 1.3385, 1.3142, 1.2918, 1.2712, 1.2517, 1.2333,

                1.2151, 1.1963,

        1.1759, 1.1524, 1.1293, 1.1192, 1.1146, 1.1114, 1.1090, 1.1069,

                1.1049, 1.1031,

        1.1014, 1.0997, 1.0980, 1.0964, 1.0949, 1.0933, 1.0917, 1.0902,

                1.0886, 1.0871,

        1.0855, 1.0839, 1.0824, 1.0808, 1.0792, 1.0776, 1.0760, 1.0744,

                1.0728, 1.0712,

        1.0696, 1.0679, 1.0663, 1.0646, 1.0630, 1.0613, 1.0597, 1.0580,

                1.0563, 1.0547,

        1.0530, 1.0513, 1.0497, 1.0480, 1.0463, 1.0446, 1.0429, 1.0412,

                1.0395, 1.0378,
```

1.0361, 1.0344, 1.0327, 1.0310, 1.0293, 1.0276, 1.0259, 1.0242,
    1.0224, 1.0207,
1.0190, 1.0172, 1.0155, 1.0137, 1.0120, 1.0102, 1.0085, 1.0067,
    1.0049, 1.0032,
1.0014, 0.9996, 0.9978, 0.9960, 0.9942, 0.9924, 0.9905, 0.9887,
    0.9869, 0.9851,
0.9832, 0.9814, 0.9795, 0.9777, 0.9758, 0.9740, 0.9721, 0.9703,
    0.9684, 0.9665,
0.9646, 0.9628, 0.9609, 0.9590, 0.9571, 0.9552, 0.9533, 0.9514,
    0.9495, 0.9476,
0.9457, 0.9437, 0.9418, 0.9398, 0.9379, 0.9359, 0.9340, 0.9320,
    0.9300, 0.9281,
0.9261, 0.9241, 0.9222, 0.9202, 0.9182, 0.9162, 0.9142, 0.9122,
    0.9102, 0.9082,
0.9062, 0.9042, 0.9022, 0.9002, 0.8982, 0.8962, 0.8942, 0.8921,
    0.8901, 0.8881,
0.8860, 0.8840, 0.8820, 0.8799, 0.8779, 0.8758, 0.8738, 0.8717,
    0.8696, 0.8676,
0.8655, 0.8634, 0.8613, 0.8593, 0.8572, 0.8551, 0.8530, 0.8509,
    0.8488, 0.8467,
0.8446, 0.8425, 0.8404, 0.8383, 0.8362, 0.8341, 0.8320, 0.8299,
    0.8278, 0.8257,
0.8235, 0.8214, 0.8193, 0.8171, 0.8150, 0.8129, 0.8107, 0.8086,
    0.8064, 0.8043,
0.8021, 0.8000, 0.7979, 0.7957, 0.7935, 0.7914, 0.7892, 0.7871,
    0.7849, 0.7828,
0.7806, 0.7784, 0.7763, 0.7741, 0.7719, 0.7698, 0.7676, 0.7654,
    0.7632, 0.7610,
0.7589, 0.7567, 0.7545, 0.7523, 0.7501, 0.7479, 0.7457, 0.7435,

```
        0.7413, 0.7391,
0.7369, 0.7347, 0.7325, 0.7303, 0.7281, 0.7259, 0.7237, 0.7215,
        0.7193, 0.7170,
0.7148, 0.7126, 0.7104, 0.7082, 0.7060, 0.7037, 0.7015, 0.6993,
        0.6971, 0.6948,
0.6926, 0.6904, 0.6881, 0.6859, 0.6837, 0.6814, 0.6792, 0.6770,
        0.6747, 0.6725,
0.6702, 0.6680, 0.6657, 0.6635, 0.6612, 0.6590, 0.6567, 0.6545,
        0.6522, 0.6500,
0.6477, 0.6455, 0.6432, 0.6410, 0.6387, 0.6365, 0.6342, 0.6319,
        0.6297, 0.6274,
0.6251, 0.6229, 0.6206, 0.6183, 0.6161, 0.6138, 0.6115, 0.6092,
        0.6070, 0.6047,
0.6024, 0.6001, 0.5979, 0.5656, 0.5933, 0.5910, 0.5887, 0.5865,
        0.5842, 0.5819,
0.5796, 0.5773, 0.5750, 0.5727, 0.5705, 0.5682, 0.5659, 0.5636,
        0.5613, 0.5590,
0.5567, 0.5544, 0.5521, 0.5498, 0.5475, 0.5452, 0.5429, 0.5406,
        0.5383, 0.5360
};


double Si410_CONVERT(double v){
    int left = 0, right = DSi410_NUM - 1;
    int mid = (left + right) / 2;
    if((v > Si410_Array[0]) || (v < Si410_Array[DSi410_NUM - 1]))
            return -1;
    while(left != right){
        if(v > Si410_Array[mid])
                right = mid;
```

```
                else

                        left = mid;

                mid = (left + right) / 2;

                if(left == mid || right == mid)

                        break;

        }

        if(Si410_Array[mid] < v){

                left = mid;

                right = mid - 1;

        }

        else{

                left = mid + 1;

                right = mid;

        }

        return (left + 1 - (v - Si410_Array[left])/(Si410_Array[right] -

            Si410_Array[left]));

}
```

Appendix C

LabWindows/CVI Programs for Stepper Motor Control

These functions control the stepper motor used in the stepper-motor-current controller.

```c
#define StepRestore WriteToDigitalLine (1, "0", 8, 16, 0, 1)        //Drive
    the motor
#define StepPulse    WriteToDigitalLine (1, "0", 8, 16, 0, 0)


#define DecreasingDirection WriteToDigitalLine (1, "0", 9, 16, 0, 0)
    //Change the direction
#define IncreasingDirection WriteToDigitalLine (1, "0", 9, 16, 0, 1)


#define LargeBoxDC_Forword   WriteToDigitalLine (1, "0", 10, 16, 0, 0)
#define LargeBoxDC_Reverse   WriteToDigitalLine (1, "0", 10, 16, 0, 1)


#define DECREASE 0
#define INCREASE 1


#define STARTATBOTTOM 1
#define STARTATTOP            0
```

```
#define TotalStep 4000        //This number is the maxium steps of
    IncreasingDirection


#define JumpStep 150


#define IntermediaTime 0.1


#define InRange (increasingsteps>=0&&increasingsteps<=TotalStep) //This
    statement is used to judge whether the slide in the limit range


int increasingsteps=0, //the totalnumber of increasing steps
    direction = 0;      //1 stands for increasing, -1 stands for dcreasing



int RunOneStep()
{
      StepPulse;
      AwareDelay(0.05);
      StepRestore;
      AwareDelay(IntermediaTime);
      increasingsteps += direction;
      return 0;
}


int RunSteps(int n)
{
      int i;
      for(i = 0;i<n;i++)
      {
```

```
            RunOneStep();
    }
    return 0;
}


int SetDirection(int b)
{
    if(b)
    {
            IncreasingDirection;
            direction = 1;
    }
    else
    {
            DecreasingDirection;
            direction = -1;
    }
    AwareDelay(1.);
    return 0;
}


int InitMotorPos(int b)    //This void is used to initial the motor
    position to the minimum
{
    if(b == STARTATBOTTOM)
    {
            increasingsteps = TotalStep;
            SetDirection(DECREASE);
            RunSteps(TotalStep);
```

```
            SetDirection(INCREASE);

            increasingsteps = 0;

    }else

    {

            SetDirection(INCREASE);


            RunSteps(TotalStep);

            SetDirection(DECREASE);

            increasingsteps = TotalStep;

    }

    return 0;

}
```

Appendix D

LabWindows/CVI Programs for PT60

This program is for the pulsed RvsT measurements in the cryostat PT60 with using the relay-diode current controller.

```c
#include <easyio.h>

#include <utility.h>

#include <cvirte.h>           /* Needed if linking in external compiler;
    harmless otherwise */

#include <userint.h>

#include "MainUI.h"

#include"DMMfun.h"

#include"Tem_Control.h"

#include"scope.h"


#define FILENAMEBRGINNING "B2_25us_"


#define NUMCURRENTS 5


#define MAXHEAT 43


static int panelHandle;


char filename[100];
```

```c
char filecurrents[NUMCURRENTS][100];

int RelaysChans[5] = {0, 2, 3, 4, 5};

double FixCurrent[NUMCURRENTS];

double InitChan1[NUMCURRENTS] = {0.2, 0.4, 0.6, 0.8, 1};
double InitChan2[NUMCURRENTS] = {1, 2, 2, 4, 4};

double heatvolt = 0., voltage, current;

int DMM1, DMM2, HeaterAddr, Pulse;

int numofdata = 10, gain1 = 10, gain2 = 1;

double Rstd = 50;
FILE * file_handle;
int Stop = 0;

int GetFileNameByTime(char *, int fieldnum);
void SetPulseAmpl(int);

int initialize(){
        char char1[100];
        DMM1 = Openit(1); //Diode Si410
        DMM2 = Openit(2); //Diode DT670
        //DMM3 = Openit(10); //sample voltage
        HeaterAddr = Openit(8); //heater address
        Scope = Openit(4);
```

```c
        //Pulse = Openit(9);

        GetFileNameByTime(filename, 0);


        intcat("TB:DEF
            EQN,'AVGS(C2)',MAXPTS,10000,SWEEPS,",char1,numofdata);
        Outit(Scope,char1);
        intcat("TA:DEF
            EQN,'AVGS(C1)',MAXPTS,10000,SWEEPS,",char1,numofdata);
        Outit(Scope,char1);
        return 0;
}


void SetHeaterVol(int intT10s, double InitVol){
        double Si410V, T;
        Set_HP6641(HeaterAddr, InitVol);
        intT10s /= 10;
        while(intT10s > 0){
                AwareDelay(10.);
                MeasureDMM(DMM1, &Si410V);
                T = Si410_CONVERT(Si410V);
                if(T > 200 || T < 0){
                        Set_HP6641(HeaterAddr, 0);
                        break;
                }
                --intT10s;
        }
}


int scanonce(int curnum){
```

```c
double resistance, current_plus, current_neg;

double uppermean, lowermean, hi1, hi2;

double Si410V, DT670V, Si410_T, DT670_T, T;

char char1[100];

//Outit(Pulse, ":PULSE:STATE ON");

//StopTrigger;

AwareDelay(1);

//autorange("C2");

//autorange("C1");

MeasureDMM(DMM1, &Si410V);

//AwareDelay(3);

Outit(Scope,"C2:TRACE OFF"); //Outit(Scope,"C4:TRACE OFF");

Outit(Scope,"TB:TRACE ON");

//Outit(Scope,"TB:FRST");

//intcat("TB:DEF

    EQN,'AVGS(C2)',MAXPTS,10000,SWEEPS,",char1,numofdata);

//printf("%s\n",char1);

//Outit(Scope,char1);

        //Turn on relay


Outit(Scope,"C1:TRACE OFF"); //Outit(Scope,"C4:TRACE OFF");

Outit(Scope,"TA:TRACE ON");

//Outit(Scope,"TA:FRST");

//intcat("TA:DEF

    EQN,'AVGS(C1)',MAXPTS,10000,SWEEPS,",char1,numofdata);

        //printf("%s\n",char1);

//Outit(Scope,char1);

//RestoreTrigger;

//AwareDelay(3);
```

```
Outit(Scope,"TB:FRST");

Outit(Scope,"TA:FRST");

AwareDelay(13);

MeasureDMM(DMM2, &DT670V);

Si410_T = Si410_CONVERT(Si410V);

DT670_T = DT670_CONVERT(DT670V);

T =  (Si410_T + DT670_T)/2.;


hi1=Get_first_cursor("C1");

hi2=Get_second_cursor("C1");

Set_param_cursors("TB", hi1, hi2);

uppermean=Get_param_mean("TB");

Set_param_cursors("TB", 0.1, 3);

lowermean=Get_param_mean("TB");


InitChan2[curnum] = uppermean - lowermean;

voltage = InitChan2[curnum]/gain2;


if(fabs(InitChan2[curnum])<20e-3)

        InitChan2[curnum] = 20e-3; //set up down limit


Set_param_cursors("TA", hi1, hi2);

uppermean=Get_param_mean("TA");

Set_param_cursors("TA", 0.1, 3);

lowermean=Get_param_mean("TA");


InitChan1[curnum] = uppermean - lowermean;

current = InitChan1[curnum]/gain1/Rstd;
```

```
        resistance = voltage/current;


        Outit(Scope,"TB:TRACE OFF");

        Outit(Scope,"C2:TRACE ON");

        Outit(Scope,"TA:TRACE OFF");

        Outit(Scope,"C1:TRACE ON");

        //ibloc(Scope);


        file_handle = safeopen(filename, "a");

        fprintf (file_handle, "%E,%E, %E,%E,%E,%E,%E, %E, %E, %E\n",

                        Days98(), heatvolt, Si410V, Si410_T, DT670V,

                           DT670_T, T, current, voltage, resistance);

        fclose(file_handle);

        PlotPoint(PANEL, PANEL_GRAPH, T, resistance, 1, 0x000000FF);

        return 0;

}


int ScanRT(){

        double maxvolt = 33.5, minvolt = 10.;

        int MaxSteps = 60, i;

        SetHeaterVol(20*60, heatvolt=maxvolt); //30mins

        for(i=1; i<=MaxSteps && Stop == 0; ++i){

                scanonce(0);

                SetHeaterVol(30,

                        heatvolt=((maxvolt-minvolt)*sqrt((1.*(MaxSteps -

                           i))/MaxSteps) + minvolt));

        }

        SetHeaterVol(0, heatvolt=0);

        return 0;
```

```c
}


int main (int argc, char *argv[])

{

        if (InitCVIRTE (0, argv, 0) == 0)    /* Needed if linking in

            external compiler; harmless otherwise */

                return -1;     /* out of memory */

        if ((panelHandle = LoadPanel (0, "MainUI.uir", PANEL)) < 0)

                return -1;

        initialize();

        DisplayPanel (panelHandle);

        RunUserInterface ();

        return 0;

}


int CVICALLBACK Quit (int panel, int control, int event,

            void *callbackData, int eventData1, int eventData2)

{

        switch (event) {

                case EVENT_COMMIT:

                        Stop = 1;

                        AwareDelay(3);

                        ibloc(DMM1);

                        ibloc(DMM2);

                        //ibloc(DMM3);

                        ibloc(HeaterAddr);

                        QuitUserInterface(0);

                        break;

        }
```

```c
		return 0;

}


int CVICALLBACK Start (int panel, int control, int event,

			void *callbackData, int eventData1, int eventData2)

{

	int num = 0;

	switch (event) {

		case EVENT_COMMIT:


				WriteToDigitalLine (1, "0", num, 16, 0, 1);

				AwareDelay(2);

				WriteToDigitalLine (1, "0", num, 16, 0, 0) ;

				break;

	}

	return 0;

}


int CVICALLBACK Scan_Once (int panel, int control, int event,

			void *callbackData, int eventData1, int eventData2)

{

	switch (event) {

		case EVENT_COMMIT:

				scanonce(0);

				//SetPulseAmpl(4.);

				AwareDelay(1);

				break;

	}

	return 0;
```

```
}

int GetFileNameByTime(char *outstr, int fieldnum) //Filename depends on
    time, date and NO. of field
{
        char timestr[9],buf[10],tempfilename[99]="";

        int i,lbuf;

        Fmt(buf,"%s<%i",fieldnum);

        lbuf = strlen(buf);

        buf[lbuf] = '_';

        buf[lbuf+1] = '\n';

        CopyString(tempfilename,0,FILENAMEBRGINNING,0,strlen(FILENAMEBRGINNING));

        CopyString(tempfilename,strlen(tempfilename),buf,0,lbuf+1);

        CopyString(tempfilename,strlen(tempfilename),DateStr(),0,10);

        CopyString(timestr,0,TimeStr(),0,8);

        timestr[8] = '\n';

        for(i=0;timestr[i] != '\n';i++){
```

```c
                if(timestr[i] != ':')


                        tempfilename[strlen(tempfilename)] = timestr[i];


        }


        CopyString(tempfilename,strlen(tempfilename),".txt",0,4);


        CopyString(outstr, 0, tempfilename,0,99);


        return 0;
}


void SetPulseAmpl(int Relays){
        int num;
        for(num = 0; num < NUMCURRENTS; ++num){
                WriteToDigitalLine (1, "0", RelaysChans[num], 16, 0, 0) ;
                AwareDelay(1);
        }
        if(Relays >= 0 && Relays < NUMCURRENTS){
                WriteToDigitalLine (1, "0", RelaysChans[Relays], 16, 0, 1);
                AwareDelay(2);
        }
}


void ScanRTvsIs(){
        double maxvolt = MAXHEAT, minvolt = 0.;
        int MaxSteps = 100, i, j;
        //init filenames for all currents;
```

```c
for(j =0; j < NUMCURRENTS; ++j){

        GetFileNameByTime(filecurrents[j], j+1);

        file_handle = safeopen(filecurrents[j], "a");


        fprintf(file_handle, "t, HV, D1V, T1, D2V, T2, T, I, V,
            R\n");
        fprintf(file_handle, "Days98, HeatVolt, d1v, T1, d2v,
            T2,T,current, voltage, resistance\n");


        fclose(file_handle);
}

//AutoAdjustAmpl(j);

SetHeaterVol(20*60, heatvolt=maxvolt); //30mins

for(i=1; i<=MaxSteps && Stop == 0; ++i){

        for(j = 0; j < NUMCURRENTS && Stop == 0; ++j){

                changerange("C1", 0.5*fabs(InitChan1[j]));

                changerange("C2", 0.5*fabs(InitChan2[j]));

                CopyString(filename, 0, filecurrents[j],0,99);

                SetPulseAmpl(j);

                scanonce(j);

        }

        SetPulseAmpl(-1);

        SetHeaterVol(50,

                heatvolt=((maxvolt-minvolt)*sqrt((1.*(MaxSteps -

                        i))/MaxSteps) + minvolt));

}

SetHeaterVol(0, heatvolt=0);

}
```

```c
int CVICALLBACK RTvsIs (int panel, int control, int event,

            void *callbackData, int eventData1, int eventData2)

{

      switch (event) {

              case EVENT_COMMIT:

                      ScanRTvsIs();

                      break;

      }

      return 0;

}
```